Available online at www.sciencedirect.com
ScienceDirect
Physics Reports 448 (2007) 133–162
PHYSICS REPORTS
www.elsevier.com/locate/physrep

Light-induced dynamics in nematic liquid crystals—a fascinating world of complex nonlinear phenomena

Gábor Demeter[a,*], Dmitry O. Krimer[b]

[a] *Research Institute for Particle and Nuclear Physics, Konkoly Thege Miklós út 29-33, H-1121 Budapest, Hungary*
[b] *Theoretische Physik, Universität Tübingen, 72076 Tübingen, Germany*

Available online 28 March 2007
editor: I. Procaccia

Abstract

Intense laser light traversing a thin layer of nematic liquid crystal is an example of a simple, easy to realise physical system, that shows very complex behaviour. Light can turn the optical axis of this uniaxial medium while propagating through it, and the dynamical behaviour that results ranges from simple orientational instabilities, through low-dimensional chaotic behaviour, to spatiotemporal pattern formation. In this paper, we review recent advances in the theoretical description of the complex phenomena that light can induce in nematic liquid crystals. We discuss the various approximations made in the models, their range of applicability, and contrast their results with experimental observations. In particular, we discuss the achievements of the plane wave approximation in various geometries, and examine how the numerous bifurcation scenarios calculated from the models can be used to interpret observations. We treat with special emphasis the results achieved in the description of the strongly nonlinear regime, where experiments have revealed interesting bifurcations and chaotic behaviour. We also discuss the mostly open problems of transverse pattern formation and the effects that can be attributed to the finite cross-section of the laser beam.

PACS: 42.70.Df; 42.65.Sf; 61.30.Gd

Keywords: Nonlinear dynamics; Nematic liquid crystals; Optical Fréedericksz transition; Optical instabilities

Contents

* Corresponding author.
E-mail addresses: gdemeter@rmki.kfki.hu (G. Demeter), Dmitry.Krimer@uni-tuebingen.de (D.O. Krimer).

0370-1573/$ - see front matter © 2007 Elsevier B.V. All rights reserved.
doi:10.1016/j.physrep.2007.02.015

1. Introduction

The optics of liquid crystals is a field whose technological importance cannot be overestimated. It stems from the enormous range of applications where liquid crystals are utilised for their ability to change their optical properties quickly in response to various electric or magnetic fields, temperature gradients, etc. The *interaction* between laser light and liquid crystals has also been investigated for long decades and is still an active field. It could be defined loosely as the subset of liquid crystal optics phenomena where the light is strong enough for its electric field to affect the liquid crystal directly, but in doing so, the propagation properties change sufficiently to induce considerable back-action on the light. This subset yields a great playground for the observation of various nonlinear phenomena, ensuring the continued interest from fundamental research. Furthermore, the area also attracted attention recently from a technological point of view in the construction of all-optical photonic switching devices.

The basic physical origin of these phenomena can be found in several review papers and monographs [1–5]. Liquid crystals are made up of elongated molecules (rod shaped, or disc shaped), with anisotropic polarisability. In a nematic liquid crystal phase, the molecular orientation is ordered, so the dielectric tensor governing the propagation of light waves is also anisotropic. The optical axis of the nematic is aligned along the local direction of the molecular axis, called the director. If the light is strong enough, its electric field, that exerts a torque on the molecules similar to any external field, is able to turn the director against the elastic restoring torques. The reorientation of the director in turn changes the optical properties of the medium that the light propagates through. A large variety of nonlinear phenomena result from this interaction. They range from simple stationary director reorientation, (the so-called light-induced or optically induced Fréedericksz transition—OFT for short), through relatively simple director precession and nutation, to low-dimensional chaos and spatio-temporal pattern formation. The optical phenomena caused by this light-induced director reorientation are sometimes referred to as the giant optical nonlinearity of nematics [1,5].

In this paper we review the latest developments in the theoretical description of these complex phenomena. The emphasis is on the description of the nonlinear domain above the optically induced Fréedericksz transition, where a multitude of different bifurcations and dynamical regimes have been observed. We discuss the various approximations that can be employed to treat the equations, discuss their applicability and usefulness, and confront theory with

experimental results. We also discuss areas where theory has not yet advanced far enough, areas which have been treated only superficially, and thus a lot of interesting observations remain largely unexplained. While our paper is concerned with the development of theory, we are bound to include a list (admittedly incomplete) of the most relevant experimental works that inspire, support, validate or invalidate the efforts of theorists.

2. Basic theoretical framework

2.1. Experimental setups

The basic experimental setup that can be used to demonstrate the interaction of nematic liquid crystals and laser light, is depicted in Fig. 1(a) and is fairly simple. A thin cell is manufactured by enclosing a nematic between two glass plates. The nematic layer is typically $L = 10$–$100\,\mu\text{m}$ thick. Since the wavelength of the light λ_{light} is in the visible range, this means that the layer is much thicker than λ_{light}. The inner sides of the enclosing glass plates are usually treated with some surfactant chemical, that orients the molecules near its surface, i.e. establishes the orientation of the director at the boundary. If this definite orientation is perpendicular to the glass plates on both boundaries, the cell is called homeotropic, if it is parallel, the cell is called planar. A hybrid cell is one where the chemicals enforce a perpendicular alignment of the molecules on one boundary, but a parallel one on the other. The cell is then irradiated with a continuous laser beam, whose light passes through the cell. The reorientation of the molecules can be monitored by analysing the outcoming light, as well as by using various probe beams, which are too weak to influence the orientation of the director themselves. The most important properties of the setup are the thickness of the nematic layer L, the material constants of the nematic, and the properties of the incident laser beam—angle of incidence, polarisation, intensity and the shape and diameter of the cross-section of the beam. The incidence angle, polarisation and beam shape are often collectively referred to as the *geometry* of the setup.

2.2. Basic equations

In the nematic phase, the molecules have some orientational order, but can move about freely as in a liquid, i.e. there is no ordering of the molecular center of mass. To describe a fluid with an orientational degree of freedom, one uses the well established hydrodynamic theory for nematics [6,7]. The starting point is the set of hydrodynamic equations for the nematic and Maxwell's equations for the propagation of light. If we assume incompressibility of the fluid, and neglect temperature differences within the medium, the relevant physical variables that these equations contain are the director field $\mathbf{n}(\mathbf{r}, t)$, the velocity field $\mathbf{v}(\mathbf{r}, t)$ and the electric field of the light $\mathbf{E}_{\text{light}}(\mathbf{r}, t)$. The generalised

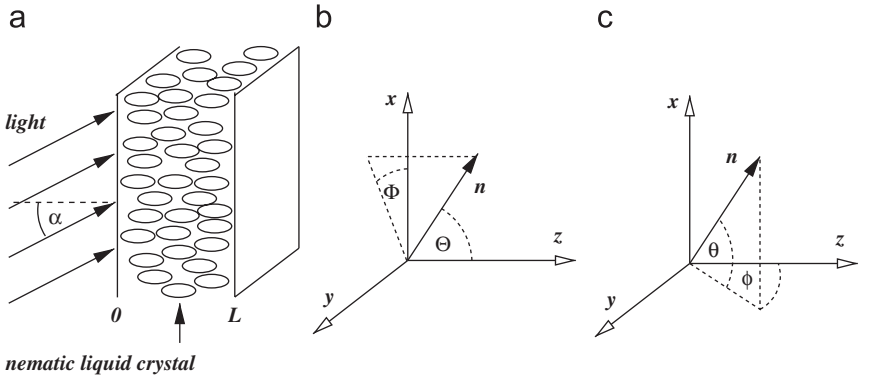

Fig. 1. (a) The basic experimental setup. A laser light with a certain polarisation is used to illuminate a cell of homeotropically aligned nematic. The light may have a nonzero angle of incidence α. The plane of the cell is usually taken to be the x–y plane, the z direction is perpendicular to it. (b) A possible description of the director using spherical angle coordinates: the polar angle Θ and the azimuthal angle Φ. (c) An alternative representation using two angle variables θ and ϕ.

Navier–Stokes equation for the velocity will be (see [6])

$$\varrho_m(\partial_t + \mathbf{v}\cdot\nabla)v_i = -\nabla_j(p\,\delta_{ij} + \pi_{ij} + T_{ij}^{\mathrm{visc}}), \tag{1}$$

where ϱ_m is the mass density and p is the pressure of the nematic. π_{ij} is the Ericksen stress tensor, which is defined as

$$\pi_{ij} = \frac{\partial F}{\partial(\partial_j n_k)}\cdot\partial_i n_k, \quad i = x, y, z. \tag{2}$$

(As usual, doubly occurring indices imply summation.) In Eq. (2) F is the free energy density, which consists of two parts. One is the elastic part

$$F^{(\mathrm{elastic})} = \frac{K_1}{2}(\nabla\cdot\mathbf{n})^2 + \frac{K_2}{2}(\mathbf{n}\cdot\nabla\times\mathbf{n})^2 + \frac{K_3}{2}(\mathbf{n}\times\nabla\times\mathbf{n})^2 \tag{3}$$

and the other is the one due to external fields, which in our case contains only the electric field of the light $\mathbf{E}_{\mathrm{light}}$:

$$F^{(\mathrm{ext})} = -\frac{\varepsilon_a}{16\pi}|\mathbf{n}\cdot\mathbf{E}_{\mathrm{light}}|^2. \tag{4}$$

Here K_1, K_2, K_3 are the splay, twist and bend elastic constants respectively [6]. $\varepsilon_a = \varepsilon_\parallel - \varepsilon_\perp$ is the dielectric anisotropy, the difference of the dielectric coefficients which describe the permittivity of the medium parallel ($\varepsilon_\parallel$) and perpendicular ($\varepsilon_\perp$) to the director. Note that $\varepsilon_\perp$ and $\varepsilon_\parallel$ depend a great deal on frequency, so in general ε_a can be positive or negative as well. However for optical frequencies, it is always positive. Any other external fields which may exert a torque on the director (static or low frequency electric or magnetic fields for example) can be included in $F^{(\mathrm{ext})}$ by adding similar terms. T_{ij}^{visc} in Eq. (1) is the viscous stress tensor:

$$-T_{ij}^{\mathrm{visc}} = \alpha_1 n_i n_j n_k n_l A_{kl} + \alpha_2 n_j N_i + \alpha_3 n_i N_j + \alpha_4 A_{ij} + \alpha_5 n_j n_k A_{ki} + \alpha_6 n_i n_k A_{kj}, \tag{5}$$

written in terms of the six Leslie coefficients α_i [8], the symmetric strain-rate tensor A_{ij}:

$$A_{ij} = (\partial_i v_j + \partial_j v_i)/2, \tag{6}$$

and the vector $\mathbf{N}$, which gives the rate of change of the director relative to the fluid:

$$\mathbf{N} = (\partial_t + \mathbf{v}\cdot\nabla)\mathbf{n} - \boldsymbol{\omega}\times\mathbf{n}. \tag{7}$$

Here $\boldsymbol{\omega} = (\nabla\times\mathbf{v})/2$ is the local fluid rotation. The six Leslie coefficients are connected by the Parodi relation $\alpha_2 + \alpha_3 = \alpha_6 - \alpha_5$ [9], so only five of them are independent. As we have assumed an incompressible fluid, the density ρ_m is constant and $\nabla\cdot\mathbf{v} = 0$.

The equation of motion for the director $\mathbf{n}$, which is also called the torque balance equation is

$$\gamma_1(\partial_t + \mathbf{v}\cdot\nabla - \boldsymbol{\omega}\times)\mathbf{n} = -\underline{\underline{\delta}}^{\perp}(\gamma_2\underline{\underline{A}}\mathbf{n} + \mathbf{h}), \tag{8}$$

where $\gamma_1 = \alpha_3 - \alpha_2$ is the rotational viscosity and $\gamma_2 = \alpha_3 + \alpha_2$. $\mathbf{h}$ is the molecular field obtained from the variational derivatives of the free energy density F:

$$h_i = \frac{\delta F}{\delta n_i} = \frac{\partial F}{\partial n_i} - \partial_j\left(\frac{\partial F}{\partial n_{i,j}}\right), \quad i = x, y, z. \tag{9}$$

The projection operator $\delta_{ij}^{\perp} = \delta_{ij} - n_i n_j$ in Eq. (8) ensures conservation of the normalisation $\mathbf{n}^2 = 1$.

The electric field which appears in the expression for the free energy density must be obtained by solving Maxwell's equations for the propagation of light. Usually we may assume a nonmagnetic material in the absence of any currents and charges, so the equations will read:

$$\begin{aligned}\nabla\times\mathbf{H} &= \frac{1}{c}\underline{\underline{\varepsilon}}\frac{\partial\mathbf{E}}{\partial t}, \quad \nabla\cdot(\underline{\underline{\varepsilon}}\,\mathbf{E}) = 0,\\ \nabla\times\mathbf{E} &= -\frac{1}{c}\frac{\partial\mathbf{H}}{\partial t}, \quad \nabla\cdot\mathbf{H} = 0.\end{aligned} \tag{10}$$

These are coupled to the hydrodynamic equations, as the dielectric tensor is given by:

$$\varepsilon_{ij} = \varepsilon_\perp \delta_{ij} + \varepsilon_a n_i n_j. \tag{11}$$

Eqs. (1), (8) and (10) are the starting point for the theoretical treatment of light-induced dynamical phenomena in nematics. Clearly, the electric field of the light appears in the director equation (8) through the molecular field (9) which contains the variational derivatives of the free energy (4). Physically, this describes an orienting torque that acts to turn the director in the direction of the polarisation. The expression for this light-induced torque can be found by performing the variational derivatives (9) on the electric part of the free energy (4):

$$\Gamma_{\text{light}} = \frac{\varepsilon_a}{16\pi}(\mathbf{E}\cdot\mathbf{n})(\mathbf{n}\times\mathbf{E}). \tag{12}$$

On the other hand, the director itself influences light propagation through the dielectric tensor (11). Furthermore, the director equation also contains an orienting torque due to elasticity (from the elastic part of the free energy density) that counteracts the light-induced reorientation of the director. Fluid flow appears in the equations, since it is coupled to the director, so director reorientation will also induce flow even in the absence of pressure gradients. This phenomenon is the so-called backflow.

The boundary conditions for the solution of this set of PDEs are usually taken to be a zero velocity due to friction between the fluid and the cell wall (the so-called no-slip condition), and a rigid orientation of the director (hard anchoring). This latter can be obtained by suitable treatment of the glass substrates, such that it ensures a rigid orientation of the molecules at the surface. In case of weak anchoring i.e. when the director is not rigidly attached to the surface, its orientation at the boundary can be taken into account by some additional surface energy terms in the free energy (3). However, dynamical phenomena induced by light appear almost exclusively in the strong anchoring case, as this is when a strong interplay between light propagation and elastic deformation takes place.

From the expression for the light-induced torque (12) acting on the director it is already evident, that a configuration where the director is perpendicular to the polarisation vector of the light (e.g. a homeotropic orientation of the director and a light field polarised in the plane of the cell) is always an equilibrium. It may be, as it happens above a certain intensity, an unstable one. This gives rise to the primary instability observed in various geometries, the much investigated optical Fréedericksz transition (OFT), whose threshold intensity in the case of linearly polarised light and perpendicular incidence is given by

$$I_F = \frac{\pi^2}{L^2}\frac{c(\varepsilon_\perp + \varepsilon_a)K_3}{\varepsilon_a\sqrt{\varepsilon_\perp}}. \tag{13}$$

It is at this point, that the light-torque prevails over elasticity and reorients the director. In situations where the initial director configuration is not perpendicular to the polarisation of the incident light, there is no such initial instability either, reorientation occurs smoothly as light intensity is increased. Note, however, that when $\varepsilon_a < 0$ (which is possible in the low frequency domain), the roles of parallel and perpendicular orientation are reversed. The latter will be stable for all field strengths and it is the former that is destabilised by the field at a certain amplitude.

2.3. Approximations

Clearly, this complex set of partial differential equations is too general to solve directly. However, there are a number of simplifications and approximations that can be applied in various situations. We will discuss the most important ones in the following. Some of these approximations are almost always valid, some have limited validity. Usually several of them are used together.

First of all, we note that the general equations contain three timescales, which differ by orders of magnitude. The time it takes the light to traverse the cell $\tau_l = L/c \sim 10^{-13}$ s, the momentum diffusion time $\tau_{\text{visc}} = \varrho_m L^2/\gamma_1 \sim 10^{-6}$ s (which is the characteristic time for the flow of the nematic) and the director relaxation time $\tau = \gamma_1 L^2/\pi^2 K_3 \sim 1$ s (which is the characteristic time for the turning of the director). The slow timescale of the system is set by the orientational viscosity of the nematic, and both flow and light propagation can be considered with the director being "fixed". The electric field of the light can thus be expressed from Maxwell's equations as a function of the instantaneous value of **n**, and can be considered as a self-consistency relation or a constraint. In a similar way, inertial terms in the Navier–Stokes

equation can be neglected and the flow of the nematic is determined entirely by the director components and their time derivatives. This separation of the timescales applies practically always.

On the other hand, the simplifications introduced by the separation of timescales still leaves us with a very complicated set of equations. The main difficulty lies in the fact that even though, $\mathbf{E}_{\text{light}}$ and $\mathbf{v}$ are theoretically defined by $\mathbf{n}$ (and $\partial_t \mathbf{n}$) at every instant t, in general the relations will be complicated integral relationships. So expressing them by $\mathbf{n}$ explicitly is not always convenient.

2.3.1. Neglection of fluid flow

One approximation that is used very often, is neglecting the flow of the nematic. Then $\mathbf{v}$ is no longer a dynamical variable, the Navier–Stokes equations can be discarded and we only need to solve the director equation (8) which will now be

$$\gamma_1 \partial_t \mathbf{n} = -\underline{\underline{\delta}}^{\perp} \mathbf{h}. \tag{14}$$

$\mathbf{h}$ will still contain the electric fields through (4) and (9), so (14) is still coupled to (10). This approximation simplifies the theoretical treatment a great deal, but it is difficult to justify rigorously in most cases. Sometimes it is possible to include flow by renormalising the rotational viscosity, but this can be done only when reorientation is small, and a linear approximation with respect to the reoriented director components is sufficient. The approximation is used much more extensively, however, with the reasoning that since flow has only a passive role (backflow), neglecting it should not cause a qualitative difference in the predictions of a theory. There are only few works where an explicit treatment of backflow has been attempted in the context of light-induced director dynamics [10–12], but there are also a number of papers, where the influence on reorientation dynamics driven by low-frequency electric fields has been considered [13–16]. These works show that in some geometries, a theory that neglects flow yields qualitatively different results from one that includes flow, i.e. it predicts different bifurcations and dynamical regimes. Usually this happens only in the strongly nonlinear regime. Then again, this is not always the case, sometimes the bifurcation scenario is the same, only the bifurcation thresholds are shifted by the inclusion of flow. Ultimately, including flow is a major complication, and often, flow is not the most essential factor in the description of the first two or three bifurcations that occur in the nonlinear regime.

2.3.2. Plane wave approximation

Another approximation that is used often is the so-called plane wave approximation. This means that the transversal cross-section of the beam is assumed to be much larger than the thickness of the cell, and the spatial dependence of all physical quantities is restricted to the coordinate perpendicular to the plane of the cell (here the z-coordinate). This approximation is (more accurately) also called the 1D approximation as only one spatial dimension is retained. (Note, however, that a wide beam with a homogeneous intensity distribution does not automatically mean that the director orientation, or any other physical quantity is also homogeneous in the plane of the cell at all times. The translational symmetry in the plane may be broken spontaneously. See Section 4.2.) The plane-wave assumption yields much simpler equations. If incompressibility is taken into account, the velocity field will be of the form $\mathbf{v} = (v_x(z,t), v_y(z,t), 0)$ and the director equations (8) reduce to (see [11])

$$\begin{aligned}
&\gamma_1 \partial_t n_x + n_z[(\alpha_2 - \gamma_2 n_x^2)\partial_z v_x - \gamma_2 n_x n_y \partial_z v_y] = -[\underline{\underline{\delta}}^{\perp} \mathbf{h}]_x, \\
&\gamma_1 \partial_t n_y + n_z[(\alpha_2 - \gamma_2 n_y^2)\partial_z v_y - \gamma_2 n_x n_y \partial_z v_x] = -[\underline{\underline{\delta}}^{\perp} \mathbf{h}]_y.
\end{aligned} \tag{15}$$

The two approximations mentioned so far are most often used simultaneously for the description of the system. The basic equations will then reduce to Eqs. (15) with the left handside simplified to only the first terms. The widespread application of the plane wave approximation is at first sight surprising. Experiments are almost never performed with laser beams whose waist size w_0 is much larger than the thickness of the cell L. Also, there is clear experimental evidence that at a certain point, the size and shape of the transversal intensity distribution becomes a very important factor [17,18]. Furthermore, there is evidence that at least in one geometry, spontaneous modulation of the reorientation profile in the transverse plane is the generic case [19,20]. However, present results suggest that the plane wave approximation does have a fairly large range of validity in the region $L/2 < w_0 < 10L$. Bellow this range, the transversal size of the laser beam is an important bifurcation parameter, and above, transversal pattern formation is expected to take place (Section 4 deals with these cases). It is notable, that most of the experiments have been performed within the range of validity

of the plane-wave approximation, and the theoretical results compare remarkably well with observations. Thus it is a very useful assumption with a fairly clear range of applicability.

2.3.3. Small reorientation

One of the most frequently used approximations in the study of light-induced director dynamics, is assuming the perturbation of the director to be small. It is then possible to simplify equations by a power series expansion in terms of the reorientation components. Unfortunately, in a lot of geometries the reorientation becomes sizeable rather quickly above the primary instability threshold. In these cases the real usefulness of such an expansion is limited to the stability analysis of the initial state (i.e. finding the primary instability). In other cases, this assumption proves useful also in the weakly nonlinear domain, even in the description of further (secondary and higher order) bifurcations. This approximation must be used with caution though, even when the director reorientation is truly small, as a power series expansion in obtaining the electric fields can have very limited validity. To show this, it is enough to see that a very important quantity, the phase shift between the ordinary and extraordinary wave components in the anisotropic medium, that is given by

$$\Delta = \frac{2\pi}{\lambda_{\text{light}}} \int_0^L \delta n \, \mathrm{d}z \tag{16}$$

depends very sensitively on the director reorientation. Since the difference of the index of refraction for the two light components δn has to be integrated over a distance $L \gg \lambda_{\text{light}}$, it can easily attain values of several times π even if the reorientation itself (and thus δn) is small. For this reason, sometimes a hybrid approach is used. Some expressions are simplified using power series expansions, but the phase shift of the waves is calculated more precisely.

2.3.4. Mode expansions

Another form of simplification comes from the typical boundary conditions that correspond to the experiments. The orientation of the director at the boundaries is usually rigid—this is called strong anchoring of the director. The spatial dependence of the director components, (or some angle variables describing the orientation of the director) can be expanded in a series of base functions that fit these boundary conditions. Typically trigonometric functions are used and obviously only a discrete set of modes (those with $m\lambda_m = 2L$) is allowed. Since elasticity in nematics introduces a damping of the mode amplitudes that is proportional to k_m^2 (where $k_m = 2\pi/\lambda_m$), higher order modes will always have a small amplitude, even in the strongly nonlinear domain. The expansion can thus be truncated at some finite number and one can trade the z-dependence of the director components for a few mode amplitudes. If, additionally the 1D assumption can also be applied, one can use the usual procedure of mode expansion and projection of the equations onto the base functions (Galerkin method) to transform the partial differential equations of motion into a set of nonlinear ordinary differential equations. Investigating the solutions of ODEs is always simpler, so such an expansion is very useful. One must take care, however, not to truncate the expansion too early, as physically important solutions can be lost. Quite often models yield a very rich bifurcation scenario—which promptly changes when adding more modes or taking into account some additional factors (like flow for example). Whenever possible, the number of modes used should be increased until a further increase no longer affects the bifurcation scenario.

It is also notable, that even when using mode expansions is not really favourable in some numerical solutions of the equations, mode amplitudes may characterise the evolution of the director much better than the numerical value of the director components at any point in space. Thus, often a projection on expansion modes follows the solution of the equations, which helps evaluation and visualisation of the results.

The essence of this method (the usage of a few scalars instead of the "infinite dimensional" functions) is often executed in a more intuitive way. An educated guess is used about the representative functional form of the reorientation with some scalar parameters, that will become "amplitudes". This trial function is then substituted into the equations of motion to obtain evolution equations for these amplitudes. Sometimes, the trial function is not a sum with the linear coefficients as parameters, but some nonlinear function (e.g. a Gaussian function with the width as a parameter).

2.3.5. The one constant approximation

The elastic energy of the nematic (3) (and the terms that arise due to it in the director equation) can be simplified a great deal by assuming all the elastic constants to be equal $K_1 = K_2 = K_3 = K$. This is known as the one-constant

approximation. Since these coefficients are material parameters that are never equal (though sometimes they are not very different,) this approximation is somewhat unphysical. It is also known to give incorrect results in certain situations, especially when transverse effects are considered (see Section 4).

2.3.6. Approximations in Maxwell's equations

The most difficult point in treating dynamical phenomena induced by light in nematics, is solving Maxwell's equations for light propagation with a sufficient accuracy. Dynamics in the nonlinear domain is driven by the interplay between director reorientation induced by light, and the change in optical properties as a result. Therefore the success or failure of a theory often depends on how this problem is tackled.

The first thing to mention is, that since director orientation is a slowly varying function on the spatial scale of the light wavelength, the electric field can always be separated into slowly varying envelope functions and fast exponentials. For example, one very convenient method is the geometrical optics approximation (GOA), where the light is divided into ordinary and extraordinary components [4,21], which propagate independently, with different phase speeds. The polarisation of the two components depends slowly on time and space only through the director components, but their magnitude remains the same. The phase exponential of the extraordinary amplitude will contain the spatially integrated index of refraction, which also depends on the director components, so usually it is a complicated expression. One can make this approach more accurate by taking into account the interaction of these waves, which is proportional to the spatial derivatives of the director components. Another method, frequently used when the plane-wave case is considered, is the Berreman approach for stratified media [22]. The electric and magnetic fields of the light can be written in the form

$$\begin{aligned}\mathbf{E}_{\text{light}}(\mathbf{r},t) &= \tfrac{1}{2}(\mathbf{E}(z,t)\mathrm{e}^{\mathrm{i}(k_x x+k_y y)}\mathrm{e}^{-\mathrm{i}\omega t}+c.c.),\\ \mathbf{H}_{\text{light}}(\mathbf{r},t) &= \tfrac{1}{2}(\mathbf{H}(z,t)\mathrm{e}^{\mathrm{i}(k_x x+k_y y)}\mathrm{e}^{-\mathrm{i}\omega t}+c.c.),\end{aligned} \tag{17}$$

with the possible x–y dependence of the fields due to oblique incidence entirely incorporated into the fast exponentials. It is straightforward to derive an equation for the amplitudes $\mathbf{E}(z,t)$, $\mathbf{H}(z,t)$ from (10), or the wave equation that can be obtained from it. A vector of four independent amplitudes describes the light field and a set of linear, first order, ordinary differential equations governs its evolution:

$$\frac{\mathrm{d}\bar{\Psi}}{\mathrm{d}z} = \mathrm{i}k_0\mathbf{D}\bar{\Psi} \quad \text{where } \bar{\Psi}^{\mathrm{T}} = (E_x, H_y, E_y, -H_x). \tag{18}$$

The matrix $\mathbf{D}$ depends on the director components [4], E_z and H_z are defined by the above four unambiguously. By calculating the eigenvalues of $\mathbf{D}$, one can separate the fast oscillations in z from the slow amplitudes.

One difficulty is apparent in both approaches: eventually, the electric field must be calculated to obtain the torque acting on the director, and it will be the superposition of the two waves with slowly varying amplitudes, but different phase factors. As mentioned before, the phase difference must be calculated very accurately, and even a small director distortion can result in a large (several times π) phase difference between the two waves. This is really the Achilles's heel for all approximate calculations. An approximation of the phase exponential (say a power series with respect to the director distortion) usually has a very limited range of validity.

2.4. On the use of computer calculations

One final remark is in order on the use of computer calculations. Because of the complexity of the equations, ultimately, all studies of light-induced nonlinear phenomena in nematics must resort to numerical integration of equations at one point or another. The question is mainly, what simplifications can be incorporated into the equations, so that the solutions still resemble the behaviour observed in the experiments. If one can reduce the complex PDEs of nematodynamics to a few explicit ODEs for some mode amplitudes, it is much easier to explore the behaviour of the system as the control parameters are varied, because a single solution with given parameters takes much less time than the solution of the original PDEs. But even more important, derivation of a "simple" model can tell us a lot about the ingredients necessary for the description of the interaction. For example, if flow, finite beam width, or twist deformations of the director are neglected in the model and it still describes the behaviour sufficiently well, we immediately have a picture on the importance (or lack of importance) of all these factors. On the other hand, if a transition to a new dynamical

regime is not shown by the simple model, we know that something that was left out does acquire decisive importance at certain control parameter values.

3. Achievements of the plane-wave theory

As mentioned in the previous section, most theoretical investigations of light-induced reorientation in nematics use the plane wave approximation. This is especially true for works treating higher order bifurcations in the strongly nonlinear domain. In what follows, we summarise the achievements obtained by these theories in several geometries.

3.1. Linear polarisation, oblique incidence

One particular geometry that has been investigated a lot, is when a linearly polarised light is incident on a cell of homeotropic nematic at a slightly oblique angle. The light is polarised perpendicular to the plane of incidence, (it is an ordinary wave), and the system thus possesses inversion symmetry with respect to this plane. (See Fig. 1(a), where the plane of incidence is the x–z plane, and the direction of polarisation is along the y axis.) Experiments revealed interesting oscillatory states in this geometry, both periodic and stochastic [23–26]. Chaotic dynamics have also been found [27], and considerable effort went into analysing this behaviour in a series of experiments [28–31].

3.1.1. Simple models

The first attempts to give a theoretical explanation [23,32] performed the linear stability analysis of the homeotropic state as a function of the angle of incidence. The treatments neglected flow, they considered the plane wave problem, employed a mode expansion and assumed the reorientation to be small, deriving the linearised equations of motion for the reorientation mode amplitudes. They showed, that as the angle of incidence grows above a certain critical angle α_{TB}, the primary instability (OFT) changes from a pitchfork bifurcation to a Hopf bifurcation. (The point where the line of a pitchfork bifurcation and a Hopf bifurcation join on a parameter plane is called a Takens–Bogdanov point—hence the subscript TB—see also Fig. 4 later on.) Thus, one may really expect to see regular oscillations above threshold for this geometry. It was also clear, however, that the critical angle of incidence above which this happens, is much larger than that used in the experiments, so the observed behaviour had to be due to higher order bifurcations.

The first serious attempt to investigate the nonlinear domain in this geometry was performed along very similar lines [33,34]. The investigation neglected flow, used the plane wave assumption and assumed the reorientation to be small. It used a mode expansion to obtain reorientation mode amplitudes, and, in extension of the linear treatment, included nonlinear terms up to third order. The director was described in terms of two angles $\mathbf{n} = (\sin\theta, \cos\theta\sin\varphi, \cos\theta\cos\varphi)$ [see Fig. 1(c)] and they were expanded in terms of sine functions as $\varphi(z,t) = \sum_n A_n(t)\sin(n\pi z/L)$, $\theta(z,t) = \sum_n B_n(t)\sin(n\pi z/L)$. The set of mode amplitudes $(A_1, \ldots, B_1, \ldots)$ were truncated, and the standard Galerkin procedure was used to obtain a set of nonlinear ordinary differential equations for the mode amplitudes. Clearly, one needs to keep at least three mode amplitudes for a "minimal model" which can possibly describe nonlinear oscillations and chaos. The most difficult point of this analysis was to express the electric fields of the light wave analytically with the mode amplitudes using Maxwell's equations. This was done using perturbation theory. The general form of the equations obtained is

$$\begin{aligned}
\tau\dot{A}_i &= \sum_j L^A_{ij}A_j + \sum_{j,k} P^A_{ijk}A_jB_k + \sum_{\substack{j,k,l\\ k\leqslant l}} Q^A_{ijkl}A_jB_kB_l + \sum_{j\leqslant k\leqslant l} R^A_{ijkl}A_jA_kA_l,\\
\tau\dot{B}_i &= \sum_j L^B_{ij}B_j + \sum_{j\leqslant k} P^B_{ijk}A_jA_k + \sum_{\substack{j,k,l\\ k\leqslant l}} Q^B_{ijkl}B_jA_kA_l + \sum_{j\leqslant k\leqslant l} R^B_{ijkl}B_jB_kB_l.
\end{aligned} \tag{19}$$

Inversion symmetry of the setup with respect to the x–z plane (the plane of incidence) implies that the equations are invariant under the transformation $S\colon\{A_i, B_i\} \to \{-A_i, B_i\}$, consequently only odd powers of the A_i-s appear in the first set of equations and only even powers in the second set. In a linear approximation, only the A_i-s have to be taken into account, as they are the ones responsible for the initial instability. Thus to obtain a "minimal model", three modes: A_1, A_2, B_1 have been retained. The resulting set of ODEs has been solved numerically, and the attracting sets that characterise the longterm behaviour (fixed-points, limit cycles, attractors) were analysed as a function of the

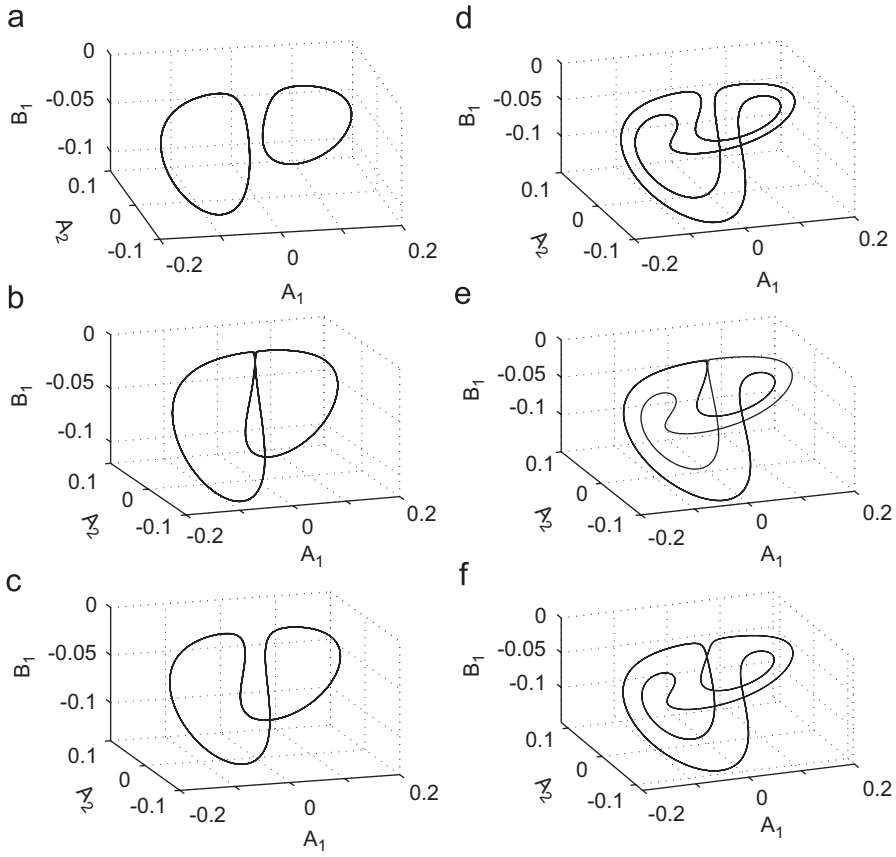

Fig. 2. Limit cycles in phase space of the three amplitudes $\{A_1, A_2, B_1\}$ at various intensities as obtained from the simple model and $\alpha = 7°$. (a) $\rho = 1.78$ two simple limit cycles, (b) $\rho = 1.80875$ the first gluing bifurcation, (c) $\rho = 1.85$ double-length limit cycle above the first gluing, (d) $\rho = 1.94$ two double-length limit cycles after the symmetry breaking instability, (e) $\rho = 1.9474$ the second gluing bifurcation, (f) $\rho = 1.96$ quadruple-length limit cycle after the second gluing.

two control parameters of the problem, the angle of incidence α and the intensity of the light normalised by the OFT threshold $\rho = I_{\text{light}}/I_{\text{OFT}}$.

The results of this "minimal model" were interesting and encouraging. In the region $\alpha < \alpha_{\text{TB}}$ where the usual optical Fréedericksz transition (the primary instability) is a pitchfork bifurcation, two new fixed points are born, which are mutual images under the symmetry transformation S. These stationary states lose stability at a slightly higher intensity in a (secondary) Hopf bifurcation, leading to a pair of limit cycles (again, mutual images under S). They are depicted on Fig. 2(a), plotted in the phase space spanned by the three amplitudes $\{A_1, A_2, B_1\}$. This result explains the regular oscillating behaviour that was observed in the experiments for $\alpha < \alpha_{\text{TB}}$. As the intensity is increased further, a very interesting scenario unfolds. The size of the limit cycles increases in phase space and they pass closer and closer to the origin (which is the homogeneous homeotropic state). At this point, this is already a saddle, not a stable fixed point. At a certain intensity ρ_1, the limit cycles become homoclinic trajectories to the origin [Fig. 2(b)] and above it, they merge to form a single, double-length limit cycle, that is symmetric with respect to S, [Fig. 2(c)]. This bifurcation is called a homoclinic gluing, or a gluing bifurcation.

As the intensity increases further, this symmetric limit cycle also looses stability, and a pair of asymmetric limit cycles are created (again, mutual images under S [Fig. 2(d)]). At a still higher intensity ρ_2, these too go through a homoclinic gluing bifurcation to form a quadruple-length, symmetric limit cycle [Fig. 2(e) and (f)]. This sequence of symmetry breaking bifurcations followed by homoclinic gluings that restore the symmetry continue ad infinitum, the length of the limit cycles doubling with each step. The bifurcation thresholds ρ_i converge to a certain value ρ_∞. Beyond this intensity, the attracting set of the dynamics is a strange attractor in phase space (Fig. 3). The system exhibits typical

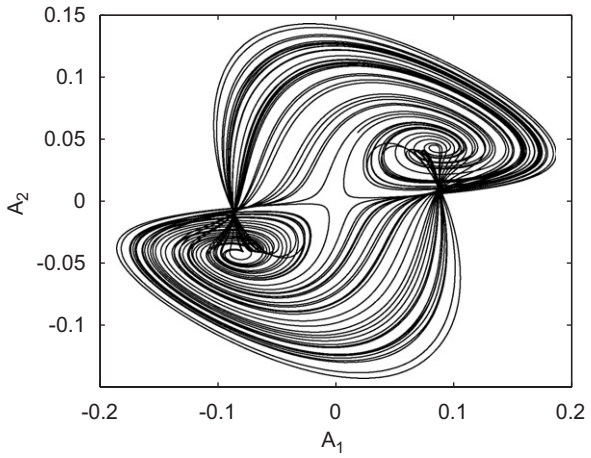

Fig. 3. Strange attractor in a subset of the phase space of the simple model at $\alpha = 7°$ and $\rho = 2.18$.

signatures of low-dimensional deterministic chaos such as great sensitivity to initial conditions and a positive Lyapunov exponent. It must be emphasised, that this route to chaotic behaviour through a cascade of homoclinic gluings is very different from the well known period doubling scenario. While it involves the birth of double-length limit cycles at a sequence of points, the period at these bifurcations diverges, as the stable homoclinic orbits at the bifurcation points have infinite periods. This distinct route to chaos was analysed in several papers [35–37], but has not yet been observed in experiment before.

The most important result of this simple model was, that the first sequence of dynamical regimes consisting of *periodic behaviour—stochastic oscillation—periodic behaviour* which was found in the experiments [27,31] could be interpreted as the evolution of the system in the vicinity of the first gluing bifurcation. In this regime, the limit cycles which are followed by the system during evolution pass close to the origin. Bellow the gluing, the two asymmetric limit cycles are very close to each other, while above the bifurcation, two segments of the same symmetric limit cycle are very close. So random fluctuations in the experiment, which are responsible for small deviations from the "ideal" limit cycle trajectory, make it possible for the system to jump from one limit cycle to the other one, or from one segment of the limit cycle to another one. Therefore one may expect to observe oscillations of the director in the vicinity of a gluing bifurcation, but with a stochastic element as random jumps take place. This is just what was observed, as two "competing" modes of oscillations. Further away from the bifurcation, the limit cycles are not close enough to the origin for the jumps to take place, so a sequence of regular oscillations, stochastic oscillations and again regular oscillations are seen as the intensity is increased. This interpretation is even more convincing if one looks at the reconstruction of the limit cycles from the experimental data [38,39], which shows clearly that the symmetry properties of the trajectories above and below the bifurcation change precisely as expected.

On the other hand, further bifurcations and dynamical regimes that were found in the experiments were not possible to interpret as the continuation of the gluing cascade. Observations showed what looked like another gluing bifurcation, but the nature of the reconstructed orbits was different from that of the limit cycles in the model around the second gluing bifurcation. Then periodic behaviour, and finally an abrupt transition to chaotic behaviour were observed. Chaos occurred at much higher intensities than in the simple model. The simple model was generalised in a natural way to include more mode amplitudes, but the discrepancies between theory and experiment remained. Still, it is notable, that the simplest possible model that could be conceived to describe the nonlinear regime, correctly predicted the first two bifurcations above the primary one. This model was also extended to include additional static fields, which were found to influence the behaviour of the system in interesting ways [34].

3.1.2. Numerical solution of the director equations

To achieve better agreement with the observations, the treatment of the simple model had to be extended. The motivation was mainly to find parameter regimes where the rare gluing cascade could be observed in the experiments. The most obvious generalisation was to extend the treatment using higher order nonlinearities. However, perturbation

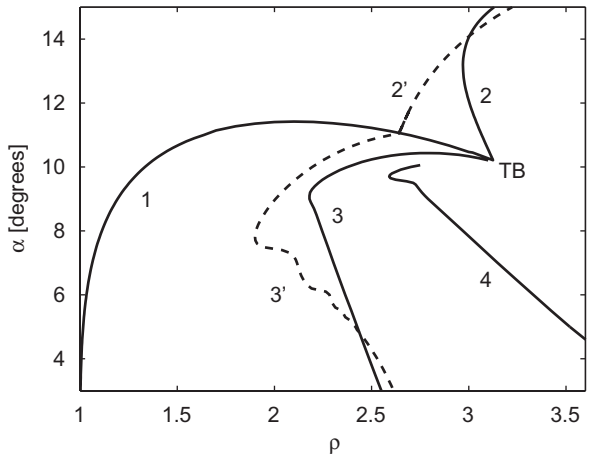

Fig. 4. Bifurcation diagram on the plane of the two control parameters: the normalised intensity ρ and the angle of incidence α. The solid lines 1 and 2 mark the primary instability, where the homogeneous homeotropic orientation becomes unstable. At 1 the bifurcation is a stationary (pitchfork) bifurcation, at 2 a Hopf one. The two lines connect in the TB point. The solid lines 3 and 4 mark the first gluing bifurcation and the second gluing bifurcation, respectively. The dashed lines 2' and 3' mark the lines of the primary Hopf bifurcation and the first gluing bifurcation when calculated without the inclusion of flow in the equations.

theory becomes far too cumbersome to use above third order, so a numerical approach was adopted, and the director equation (14) was solved using a finite difference discretisation method [40,41]. This approach has the advantage that nonlinearities of arbitrary order are retained in the director components, which is especially important when solving Maxwell's equations. As also noted later in [42], the primary reason why the simple model looses its validity at fairly low intensities is, that the perturbative solution of the light propagation equations fails at not too high reorientation amplitudes. The numerical treatment still neglected flow, and used the plane wave approximation.

The results obtained from this calculation were somewhat puzzling. While the first two bifurcations above the primary instability (the secondary Hopf-bifurcation and the first gluing bifurcation) were found to occur as in the simple model, the full cascade of gluing bifurcations were not found at all at any parameter values. Furthermore, chaos was found only in parameter regions that did not correspond to the experimental setups used in [38,39,31] This study made it clear that although higher order nonlinearities with respect to the director components give an important contribution to the dynamics, they are not the only essential ingredients.

3.1.3. Numerical solution of the nematodynamical equations

In further pursuit of the elusive gluing cascade, one clearly had to refine theory to achieve better correspondence with observations by including either a proper treatment of the nematic flow, or by discarding the plane wave approximation. The choice was to include flow in the theory, and retain the plane wave approximation. This was motivated by findings that the cross section of the beam becomes an important ingredient in the nonlinear behaviour only when its size is about half of the cell thickness (see Section 4.1). The numerical study of the full nematodynamical equations was thus performed [12] along similar lines as the previous one. This time, the results were much closer to the observations. The first three bifurcations (the optical Fréedericksz transition, the secondary Hopf- and the first gluing bifurcation) were found in the simulations just as before. The lines of the primary instability and the first gluing bifurcation on the ρ–α plane are shown in Fig. 4. They are depicted as calculated from both simulations, (the one without flow and the one including flow), to show the quantitative difference between the bifurcation thresholds.

However, using parameters that correspond to the experiments, the next bifurcation was not the second gluing found in the simple model. As the intensity increased, the symmetric limit cycle was found to break up into the two simple limit cycles depicted on Fig. 2(a), in what could be called an inverse gluing (or ungluing) bifurcation. After this second gluing bifurcation, there is periodic behaviour until chaos appears abruptly at a certain intensity. This sequence now is perfectly compatible with the behaviour observed in the experiments at all intensities, apart from some quantitative differences in the bifurcation thresholds. The calculations thus showed that flow is an important ingredient of the

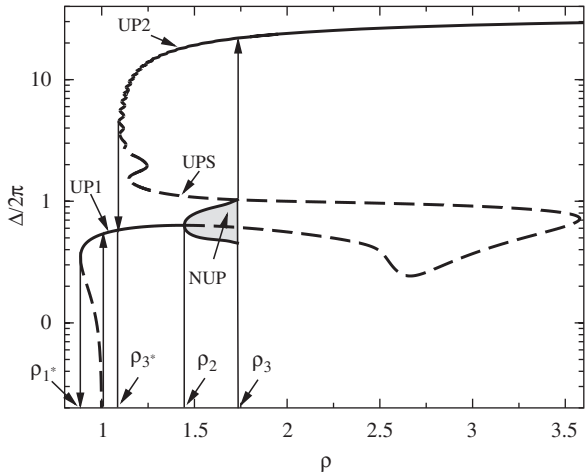

Fig. 5. Bifurcation diagram of a nematic distorted by CP light, showing the phase delay $\Delta/2\pi$ versus normalised intensity ρ in semi-logarithmic scale. The lines mark the reorientation amplitude of various limit-cycle solutions. Solid (dashed) lines mark stable (unstable) states and the gray region refers to the NUP regime.

nonlinear behaviour at high intensities, and supported the assumption that finite beamsize effects are not of qualitative importance when $w_0 \approx L$.

The last thing worth mentioning is, that in the calculation with flow a parameter region was found where the gluing cascade does exist. This region is close to the TB point, and the bifurcation lines are nearly parallel to the ρ axis, so they can be traversed by keeping the intensity fixed and decreasing the angle of incidence. The cascade is located in a region that lies outside the experimentally explored one, so its existence is yet to be confirmed. It is, however, a very exciting prospect.

3.2. Circular polarisation, perpendicular incidence

Another interesting geometry which has been studied very intensively, both experimentally and theoretically, is where a circularly polarised light beam is incident perpendicularly on a layer of homeotropically oriented nematic. This geometry is interesting partly because it is one of the earliest configurations where light induced dynamical behaviour was observed. But more importantly, it is a geometry where relatively simple models proved to be efficient in describing some of these phenomena, and giving a simple physical picture of their origins.

In this geometry, the OFT was found in the experiments to be a first order transition (i.e. a subcritical bifurcation), with a well detectable hysteresis cycle and bistability as the light intensity was changed. Above the threshold the molecules undergo a collective rotation [43] that corresponds to a uniform precession of the director (see the UP1 branch of the bifurcation diagram in Fig. 5). The threshold intensity is twice that needed for the linearly polarised case. (A circularly polarised light is composed of two independent linearly polarised ones. For any small director deviation from the initial state, only one of these components will exert a torque on the director, because the other will still be perpendicular to it. Since the energy the light carries is divided evenly between the components, and one component must be intensive enough to reorient the nematic by itself, the threshold intensity for CP light is double that of the linearly polarised case.)

Both director precession, and the first order nature of the transition could be explained in intuitive ways [43–45]. The precession of the director is caused by the fact that once it reorients, the relative phase of the two linear components that make up the circularly polarised beam changes as light propagates through the layer. The ordinary wave will propagate at the same speed as before, but the extraordinary wave will experience a different index of refraction, and thus propagates with a different speed. The change of the relative phase means that light will become elliptically polarised, and the director starts turning towards the major axis of polarisation, which causes a steady precession. The subcriticality of the transition is also due to the light becoming elliptically polarised. The OFT threshold intensity for elliptically polarised light is smaller than for circularly polarised light (see Section 3.3), so once light acquires elliptical

polarisation, it can support director reorientation against elasticity down to an intensity that is bellow the original OFT threshold. It is worth noting, that due to isotropic symmetry of the setup in the plane of the layer, rotating states are in fact the generic solutions that one may expect. They are also called Goldstone modes and are related to the spontaneous breaking of the isotropic symmetry by the OFT (see e.g. [46,47]). A stationary reoriented state would be the special case of zero frequency.

Interestingly, the steady precession of the molecules after director reorientation also has a clear "quantum" interpretation, as being due to spin angular momentum transfer from the light to the medium (the so-called self-induced stimulated light scattering [44]). To transform circularly polarised light incident on the transparent liquid crystal medium into an elliptically polarised one that exits the cell, some photons must be scattered into an opposite helicity state, i.e. their spin must be reversed. A constant deposition of spin angular momentum to the medium means a constant torque acts on the director, that balances the viscous torque arising from director motion. The energy that the rotating molecules dissipate due to viscosity is supplied by the slight red-shift of the scattered photons.

3.2.1. Simple models

The peculiarities of the OFT in this geometry discussed qualitatively above are recovered by simple models [45,48]. The key approximations these models use are (i) the plane-wave approximation and the assumption that all variables depend on the z coordinate only, (ii) flow is neglected, (iii) the reorientation is assumed to be small and (iv) the slow-envelope approximation is used for Maxwell's equations. It is convenient to consider the problem in the usual spherical angles $\Theta(z,t)$ and $\Phi(z,t)$ such that $\mathbf{n}=(\sin\Theta\cos\Phi, \sin\Theta\sin\Phi, \cos\Theta)$ [see Fig. 1(b)]. The azimuthal angle $\Phi=\Phi_0(t)+\Phi_d(z,t)$ can be decomposed into two parts, where $\Phi_0(t)$ is a rigid rotation of the director around the z axis (no distortion), and Φ_d is the twist distortion. The importance of this decomposition is, that in general, Φ_0 cannot be assumed to be small even if the reorientation itself is tiny. The smallness of the reorientation implies that the splay-bend, and the twist distortions are small, (i.e. $\Theta^2(z,t)\ll 1$ and $|\partial_z\Phi_d|\ll 1/L$, respectively), but not Φ_0 itself. The models also used a mode expansion for Θ with just one sine mode (i.e. $\Theta\sim\sin(\pi z/L)$) and the model of [48] also used a one mode approximation for Φ_d. The models then employed power series expansions with respect to the mode amplitudes.

As expected, these models describe very well the initial instability, the stable precession regime and its hysteresis cycle (the UP1 branch in Fig. 5). The model of [45], which has been derived by retaining terms up to third order in Θ and only to the lowest order in $\partial_z\Phi_d$ in the corresponding nonlinear operator $\mathbf{h}$ from Eq. (14), goes even further. It predicts the existence of a second precession regime (with a large reorientation amplitude) that has been seen in the experiments. The transition is discontinuous with a large hysteresis loop (see the UP2 branch in Fig. 5). The frequency of the precession in the second regime was found to be at least one order of magnitude smaller than for the first regime and to exhibit rapid variations with the incident intensity, reaching zero at roughly periodic intervals. These properties are also recovered from the model, which predicts the precession frequency to be

$$f_0\tau=\frac{\rho(1-\cos\Delta)}{2\pi\Delta}. \tag{20}$$

Here ρ is the normalised intensity, and τ the director relaxation time as before. Δ is the phase delay between the ordinary and extraordinary waves induced by the whole layer (see Section 2.3.3). This quantity is very suitable for an overall characterisation of the magnitude of reorientation, because it is directly measurable—$\Delta/2\pi$ represents the number of self-diffraction rings in the far field [49]. It is worth noting that this model describes the second regime rather well, even though the angle Θ is large there, which actually contradicts the initial assumption.

3.2.2. Extension of the simple model

The success of the simple approximate models (in particular the agreement with contemporary experiments) shifted attention from this geometry, until some years later, a secondary instability between the OFT and the abrupt transition to the largely reoriented state was observed [50]. A theory to describe this intermediate transition was attempted [51], and eventually successfully constructed [52,53]. For this purpose the angles Θ and Φ_d were expanded in systems of orthogonal functions which satisfy the boundary conditions: $\Theta=\sum_{n=1}^{\infty}\Theta_n(t)\sin nz$, $\Phi_d=\sum_{n=1}^{\infty}\Phi_n(t)\sin(n+1)z/\sin z$. (Here $z=z'\pi/L$ a normalised coordinate.) These studies improve the simple models basically by taking more modes to describe the reorientation angles (namely six modes for each angle were found to be enough), and by relaxing the assumption that the reorientation is small. Neglection of flow and the plane wave approximation were retained. The expansions were used to obtain a set of nonlinear ODEs for the reorientation amplitudes Θ_n and Φ_n via the standard

Galerkin method. Since expansions of this complexity did not allow any parametric solution of Maxwell's equations, they were simulated dynamically with computers at every step of the time integration.

Numerical solutions of the extended model confirmed the scenario near the OFT. The OFT transition occurs at $\rho = 1$ and is subcritical. Once the director settles to the UP1 state and the intensity is decreased, the director switches back to the homeotropic state at some lower value of intensity $\rho = \rho_1^*$ where a saddle-node bifurcation occurs (see Fig. 5). For the UP1 state, the phase delay that can be used to characterise the reorientation amplitude is $\Delta \approx \pi$. The trajectory of the director in the (n_x, n_y) plane in the laboratory is a circle, whereas in a frame rotating with frequency f_0 around the z axis it is a fixed point.

One should make an important remark concerning the nature of the OFT at this point. Strictly speaking the answer to the question whether the transition is sub- or supercritical must be obtained from a weakly nonlinear analysis. The latter gives the following criterion [53]: the transition is supercritical (subcritical) if the coefficient $C = K_1/K_3 - (9/4)(\varepsilon_a/\varepsilon_{||})$ is positive (negative). This criterion is identical to the one derived in the case of OFT under linearly polarised light [54]. In the calculations of [53], C turns out to be 0.154 and the OFT is thus expected to be supercritical, which seems to contradict the results of the simple models and observations. The precise numerical solution shows, that the OFT is indeed supercritical in the present example but the solution branch turns over and becomes subcritical (and unstable) already at $\rho = 1 + \delta\rho$ where $\delta\rho \simeq 10^{-6}$, which is too small to detect.

As the intensity increases further, the UP1 state becomes unstable at an intensity $\rho = \rho_2$ where the director starts to nutate (NUP regime). This transition was identified as a supercritical Hopf bifurcation. The phase delay Δ starts to depend on time in this regime and is represented by a gray region in Fig. 5. (The upper and the lower lines limiting this region are the maximal and minimal values taken by Δ during its oscillation.) Whereas the trajectory of the director in the laboratory frame is not closed (the motion of the director is quasiperiodic), the director performs a simple periodic motion with a frequency f_1 in the frame that rotates with a frequency f_0 around the z axis [see Fig. 6(a),(b)].

The NUP state in turn looses stability at $\rho = \rho_3$ where the system jumps to a new state of uniform precession of the director (UP2) with large reorientation and slow precession frequency. Starting from the stable UP2 branch above ρ_3 and lowering the excitation intensity, one finds a large and rather complicated hysteresis cycle which consists of alternatively stable and unstable regions exhibiting a series of saddle-node bifurcations (predicted also by the simple model [45]). The system eventually switches back to the UP1 solution at ρ_3^* (see Fig. 5). The UPS branch, which is an unstable, uniform precessing state, constitutes the separatrix between the basin of attraction of the stable UP2 and the stable NUP states (or, below ρ_2, the UP1 state). In a reference frame rotating with f_0, the UPS state is a saddle point, and the transition from the NUP regime to the UP2 state happens when the NUP limit cycle becomes homoclinic to this saddle. Thus the transition at $\rho = \rho_3$ is a homoclinic bifurcation of the simplest type where a limit cycle collides with a saddle point having only one unstable direction [57]. Fig. 6(c), (d) illustrates convergence of the trajectory to the NUP state bellow ρ_3 from various initial conditions.

All theoretical findings discussed up to now agree qualitatively with experiments [53]. However, there were still quantitative discrepancies, for example, the measured onset of the nutation-precession motion was found to be about 20% lower than predicted by theory.

3.2.3. *The effects of flow*

In an attempt to see if quantitative differences between experimental results and theoretical predictions were due to the neglection of flow, or the plane wave approximation, a study was performed with the inclusion of backflow [11]. For this purpose the coupled director and Navier–Stokes equations have been solved which, after adiabatic elimination of the flow field reduce to Eqs. (15). From the linear stability analysis of the basic state follows that the threshold for the OFT is unchanged, whereas the growth rate $\sigma = (\rho - 1)/(\tau\xi)$ acquires a "linearised viscosity reduction factor" $\xi < 1$ ($\xi = 1$ corresponds to neglection of backflow). This factor is given by $\xi = 1 - (1 - 8/\pi^2)\,\alpha_2^2/\eta_2$, where $\eta_2 = (\alpha_4 + \alpha_5 - \alpha_2)/2$ is an effective viscosity and α_i are Leslie coefficients [6]. The expression for ξ accidentally coincides with that obtained in [10] where a one-mode approximation for the director components and smallness of the twist distortion were used.

In [11] the dynamic equations for Θ and Φ (which are much more complicated than those derived without the inclusion of flow) have been simulated by using of the same (Galerkin) method described in Section 3.2.2. In Fig. 7 the results of calculations of the phase delay for the case with and without flow are compared with each other. It turns out that backflow does not lead to qualitative changes in the dynamical scenario, but does lead to substantial quantitative changes in the secondary bifurcation threshold. Namely, the onset of nutation is shifted towards higher value of intensities by about 20% and exists in a larger interval. As is seen from Fig. 7 the thresholds for the NUP and

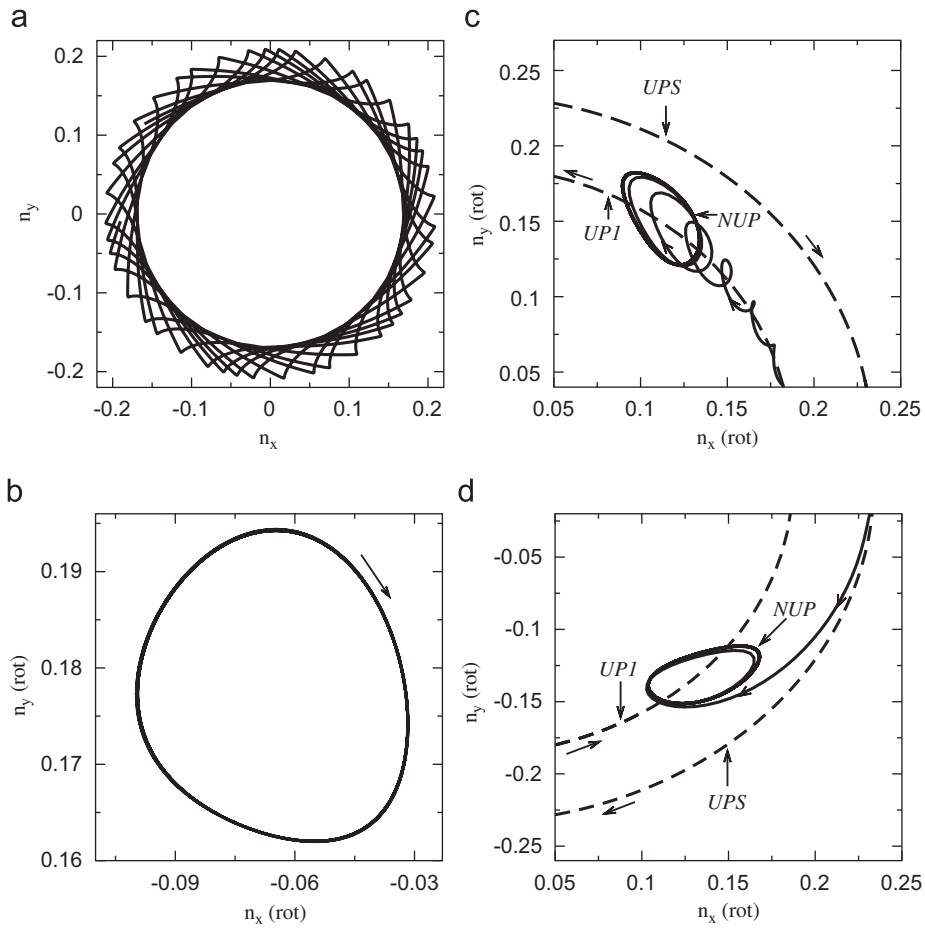

Fig. 6. (a),(b) director trajectory at $\rho = 1.55$. (a) Quasiperiodic behaviour in the laboratory frame (n_x, n_y). (b) Periodic limit cycle in the rotating frame $(n_x^{\mathrm{rot}}, n_y^{\mathrm{rot}})$. The arrow indicates the sense of rotation when the incident light is left circularly polarised. The sense of rotation is always opposite to that of the underlying precession [55]. (c),(d) director trajectory at $\rho = 1.55$ in a frame rotating with f_0, showing the instability of the UP1 and UPS solutions in the NUP regime. (c) Initial condition near the UP1 solution. (d) Initial condition near the UPS solution. The arrows indicate the sense of rotation of the corresponding trajectory when the incident light is left circularly polarised.

for the UP2 regimes turns out to be $\rho_2 = 1.75$ and $\rho_3 = 2.4$ instead of $\rho_2' = 1.45$ and $\rho_3' = 1.75$ when the backflow is neglected [52,53]. It is worth noting that the precession frequency f_0 for UP1 states increases when the backflow is included. Such a behaviour is expected because γ_1 effectively decreases.

Unfortunately, the inclusion of backflow did not diminish the quantitative discrepancy between theory and experiment. (The experimental values of the thresholds ρ_2, ρ_3 are even smaller than that given by the theory without backflow [52,53].) One is forced to conclude that the discrepancy is mainly due to the plane wave approximation, and to improve the correspondence with the experiment one has to include the lateral degree of freedom.

3.3. Elliptic polarisation, perpendicular incidence

The case of an elliptically polarised (EP) light inducing the director reorientation is a logical generalisation of the linearly and circularly polarised cases, which has also been investigated in depth. EP light is characterised by the ellipticity χ, which is related to the ratio of the minor and the major axis of the polarisation ellipse and lies in the interval $[-\pi/4, \pi/4]$. The case $\chi = 0$ ($\chi = \pm\pi/4 \simeq \pm 0.785$) corresponds to a linearly (circularly) polarised light. The sign of χ determines the handedness of the polarisation (left or right), thus it is sufficient to choose $\chi > 0$ only. Clearly, the rotational invariance around the z-axis for EP light is broken.

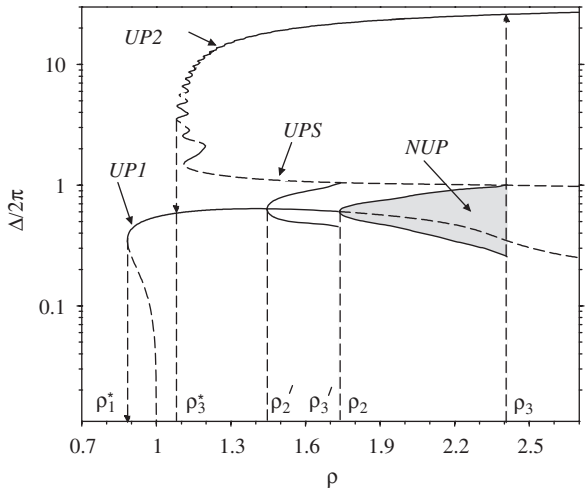

Fig. 7. Bifurcation diagram of a nematic distorted by CP light, showing the phase delay $\Delta/2\pi$ versus normalised intensity ρ from two different calculations, one which includes flow and one that does not. The lines mark the reorientation amplitude of various limit-cycle solutions. Solid (dashed) curves correspond to stable (unstable) UP solutions. Gray region: nonuniform precession states of the director. Dash-dotted lines in the (ρ_2', ρ_3') interval: nonuniform precession states of the director when backflow is neglected. The fact that $\rho_3' \simeq \rho_2$ is accidental.

The first step, as usual, is the linear stability analysis of the unperturbed (U) state. Again, the same assumptions (i)–(iv) mentioned in Section 3.2.1 can be used here. In [58] the threshold intensity of the OFT for arbitrary χ was shown to be given by the formula $I_F^{\mathrm{EP}} = I_F^{\mathrm{CP}}/(1+\cos 2\chi)$, where I_F^{CP} is the threshold intensity of the OFT for CP light. This is depicted by the lowest solid line in Fig. 8 in the (χ, ρ) plane, where the intensities are normalised as $\rho = I/I_F^{\mathrm{CP}}$.

For fixed ellipticity χ and with increasing light intensity ρ the system switches to a stationary distorted state (D) at the OFT for all ellipticities $\chi < \pi/4$, except the circular case $\chi = \pi/4$. With further increase of the intensity, an oscillating state (O) was experimentally observed [59]. The numerical analysis [59] of the basic equations indeed predicts the existence of such a state. In a later study, rotating states have been experimentally found [60]. A relatively simple model was then proposed in [60] to describe all essential features of the director dynamics for not too high values of ρ. A full numerical study was performed in [61] to clarify the director dynamics at higher intensities, which cannot be reproduced by the simple model.

3.3.1. Simple model

The main assumptions used for the derivation of the simple model for EP light [60] are the same as those used for the CP case, namely the plane wave approximation without flow and the assumptions of small reorientation and slow envelope approximation for the light (see Section 3.2.1). Again both the polar and the twist angles were assumed to be small ($\Theta^2 \ll 1$ and $\Phi_d \ll 1$). All nonlinear operators were expanded with respect to these angles and only few significant nonlinear terms were kept. Then a mode expansion for Θ and Φ was used and only the first mode Θ_1 for the polar angle was retained. The field equations were solved iteratively using the twist angle as a small parameter. The first iteration was taken as an approximate solution for the field amplitudes. Finally, the problem reduced to a set of two ODEs for the phase delay Δ (which is proportional to Θ_1^2 within this approximation) and the zeroth mode Φ_0 (which represents a rigid rotation, as before). The twist modes $\Phi_{n\geqslant 1}$ were assumed to follow adiabatically their steady state values and were shown to decrease rapidly with n, so only a few of them were important. Interestingly, if all twist modes are neglected no oscillations of the director can be obtained. So the twist degrees of freedom are essential to induce the nonlinear oscillations [60].

This relatively simple model was capable of predicting not only O states but also some other states occurring at higher intensities. In particular, it was shown that the transition from D to O states takes place via Hopf bifurcation, while the transition from oscillation to rotation was shown to be the gluing of two symmetrical limit cycles. The hysteresis between rotations and oscillations at large ellipticity χ observed in the experiment [60] was also predicted by the model.

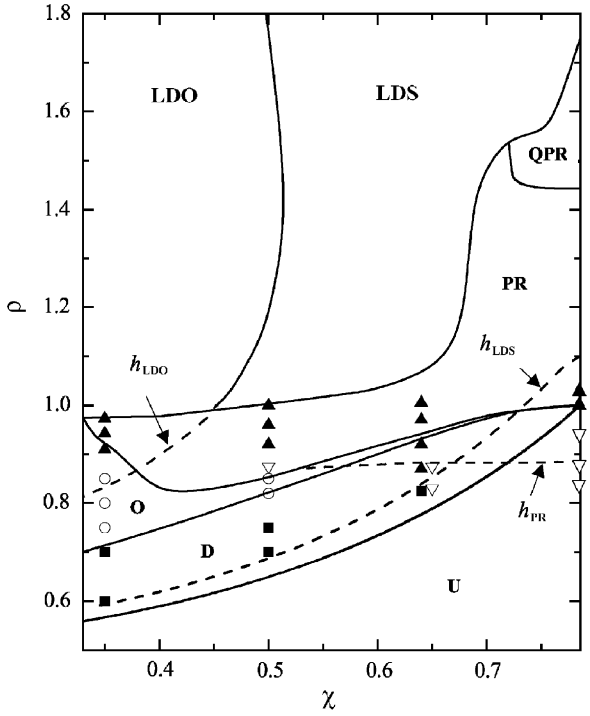

Fig. 8. Phase diagram of the dynamical regimes in the parameter plane (χ, ρ). U: Undistorted state; D: stationary distorted states; O: periodic oscillating states; PR: periodic rotating states; QPR: quasi-periodic rotating states; LDS and LDO: stationary distorted and oscillating states, with a large reorientation. The dashed lines h_{PR}, h_{LDS} and h_{LDO} correspond to the region of hysteresis for the PR, LDS and LDO states, respectively. The points are experimental data extracted from [60] for D (■), O (○), PR (▲) and hysteretic PR (▽).

3.3.2. Numerical study

A new interest in the problem of EP light arose after the discovery of the quasiperiodic director rotation (QPR) for CP light and the successful theoretical description of this phenomena (see Section 3.2, where this regime has been called the NUP regime). This new regime appears in the CP case, if the incident intensity exceeds the one for the OFT by about 40% (calculated without backflow). This lies already outside the region of intensities investigated in [60]. Since in the experiment there is always a certain amount of residual ellipticity (i.e. it is not possible to prepare the ideal circular polarisation), it became interesting to investigate, just how sensitive the director behaviour is in the vicinity of this new bifurcation when mismatching from the CP case. So the logical aim was to complete the bifurcation map in the (χ, ρ) plane. This could not be done in the context of the simple model, as it fails for higher intensities because (i) the assumption about the smallness of the director distortion becomes incorrect and (ii) higher order nonlinearities in twist terms $[\propto (\partial_z \Phi_d)^2]$ that were neglected in the model become important. To this end, a numerical study of the equations was performed, along similar lines as that described in Section 3.2.2.

In [61] the QPR regime for EP light was found both theoretically and experimentally for the region of ellipticities close to the CP case. There, the map of dynamical regimes from moderate to large ellipticities $(0.33 \leqslant \chi \leqslant \pi/4)$ has been constructed that is shown in Fig. 8. (For smaller χ the map looks similar to that obtained in the simple model of [60].) Keeping the ellipticity fixed and increasing the intensity, these regimes appear as a well-defined sequence of transitions as is summarised in Table 1. The trajectories of the director in various regimes are shown in Fig. 9. Above the OFT threshold several different regimes can exist depending on the values of χ and ρ: stationary distorted (D), oscillating (O), periodic rotating (PR), quasi-periodic rotating (QPR) and largely reoriented states ($\Theta \sim 1$). The latter may be stationary distorted (LDS), oscillating (LDO) or rotating (LR) states.

The OFT is a pitchfork bifurcation and the reoriented state is a D state (see the filled circles in Fig. 9). This state loses its stability through a supercritical Hopf bifurcation to an O state [curve 1 in Fig. 9(a)] characterised by a single frequency f_0. It should be noted that reflection symmetry is spontaneously broken by the first bifurcation, so in the D

Table 1
Calculated sequence of bifurcations as a function of the ellipticity χ of the incident light

Ellipticity	Sequence of transitions	Bifurcation nature
$0.33 < \chi < 0.53$	Unperturbed → Distorted	Pitchfork
	Distorted → Periodic oscillation	Supercritical Hopf
	Periodic oscillation → Periodic rotation	Gluing
	Periodic rotation → Periodic oscillation or distorted	Homoclinic[a]
$0.53 < \chi < 0.72$	Unperturbed → Distorted	Pitchfork
	Distorted → Periodic oscillation	Supercritical Hopf
	Periodic oscillation → Periodic rotation-1	Gluing
	Periodic rotation-1 → Periodic rotation-2	Saddle-node
	Periodic rotation-2 → Distorted	Homoclinic[b]
$0.72 < \chi < \pi/4$	Unperturbed → Distorted	Pitchfork
	Distorted → Periodic oscillation	Supercritical Hopf
	Periodic oscillation → Periodic rotation-1	Gluing
	Periodic rotation-1 → Periodic rotation-2	Saddle-node
	Periodic rotation-2 → Quasi-periodic rotation	Supercritical Hopf
	Quasi-periodic rotation → Distorted or periodic rotation	Homoclinic[c]
$\chi = \pi/4$	Unperturbed → Periodic rotation	Subcritical Hopf
	Periodic rotation → Quasi-periodic rotation	Supercritical Hopf
	Quasi-periodic rotation →Periodic rotation	Homoclinic[c]

[a]Small jump of the director amplitude.
[b]Small [large] jump of the director amplitude for $\chi < 0.66$ [$\chi > 0.66$].
[c]Large jump of the director amplitude.

and O states one has two symmetry degenerate solutions related by $\{n_x \to -n_x, n_y \to -n_y\}$. As ρ increases, these two limit cycles merge in a gluing bifurcation at the origin and restore the reflection symmetry. This leads to the appearance of a single double-length limit cycle that corresponds to the trajectory in the PR state (curve 2 in Fig. 9). (Note that for $\chi < 0.33$ the rotating state is suppressed, see [61] for more details.)

For $\chi > 0.53$, there is an additional bifurcation between PR states (not shown in Fig. 8 because it is very close to the gluing bifurcation). The amplitude of the PR state occurring just above the gluing, now labeled PR_1 [curve 2 in Fig. 9(b),(c)], abruptly increases giving rise to another periodic rotating state labeled PR_2 with higher reorientation amplitude [curve 3 in Fig. 9(b),(c)]. This is a hysteretic transition which has a double saddle-node structure separating the PR_1 and PR_2 branches. (This feature was already found in the framework of the approximate model [60].) If the director settles in the PR_2 state and the intensity is decreased, the system switches back to the O or D state at the line labeled h_{PR} in Fig. 8. Note that at $\chi = 0.53$ the two saddle nodes coalesce.

A further increase of the intensity eventually leads to a discontinuous transition via homoclinic bifurcation to LDO state ($0.33 < \chi < 0.45$) or LDS state ($0.45 < \chi < 0.72$). This transition is associated with a small (large) relative jump of the director amplitude for $\chi < 0.66$ ($\chi > 0.66$). If one starts from the LDO state and the intensity ρ is decreased, the amplitude of oscillations goes to zero leading to the LDS state (see the hysteretic line h_{LDO} in Fig. 8). This LDS state, in turn, vanishes if the intensity is decreased below the hysteretic line h_{LDS}.

For $0.72 < \chi < \pi/4$ the PR_2 state looses stability via supercritical Hopf bifurcation (as ρ increases) and the system acquires a new frequency f_1 which leads to the QPR state [curve 4 in Fig. 9(c)]. As the intensity increases further the QPR state undergoes a homoclinic transition to the LDS or LR state. The latter arises only in a narrow region $\Delta\chi \sim 10^{-2}$ near $\chi = \pi/4$ and is not shown on Fig. 8.

The QPR regime has been observed in the experiment and was shown to exist in a narrow region of ellipticities close to circular polarisation [61] as predicted by theory. However, a quantitative agreement was not achieved which means that one should refine the theory by including backflow and finite beam size effect. One expects the dynamical scenario to remain qualitatively the same after such refinements however, as the inclusion of flow did not change the picture in the CP case, and the beam size proves decisive only when it is significantly smaller than L (see Section 4.1).

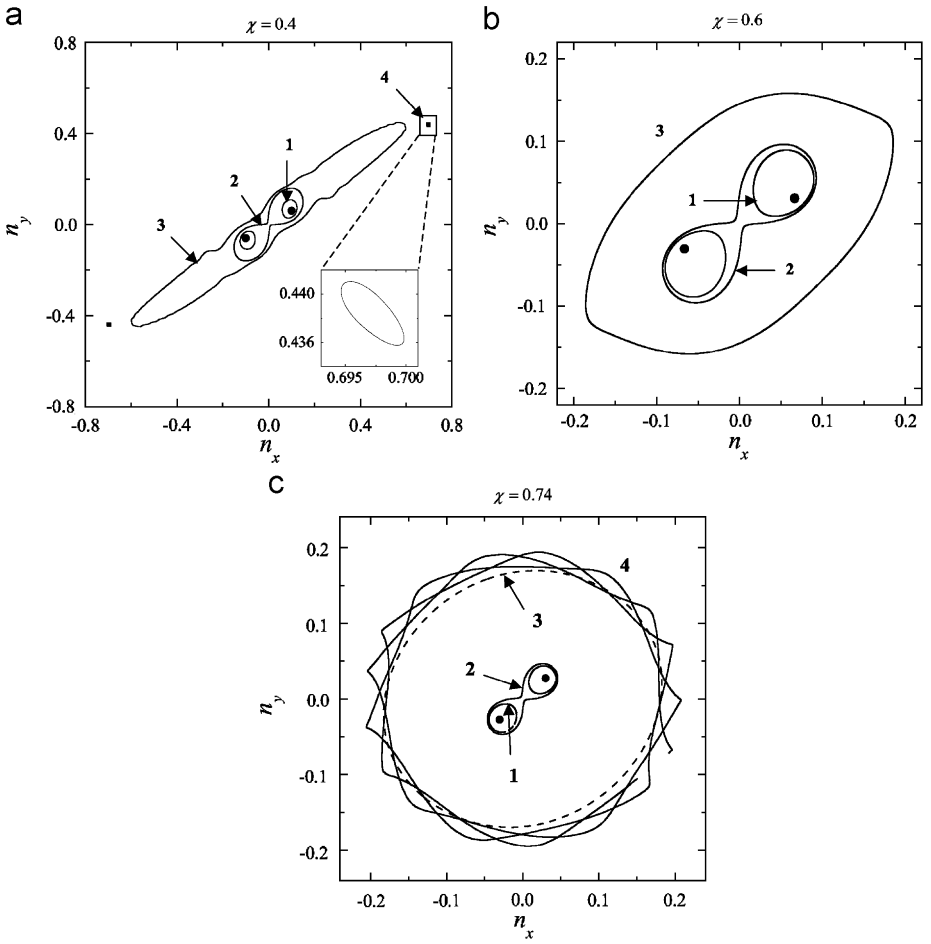

Fig. 9. Calculated director trajectories in the (n_x, n_y) plane. (a) $\chi = 0.4$: stationary distorted state (D) at $\rho = 0.72$ (•); periodic oscillating state (O) at $\rho = 0.76$ (curve 1); periodic rotating state (PR) just above the gluing bifurcation at $\rho = 0.83$ (curve 2) and slightly below the transition to the largely reoriented oscillating state (LDO) at $\rho = 0.97$ (curve 3); largely reoriented oscillating state at $\rho = 0.98$ (curve 4, see inset). (b) $\chi = 0.6$: stationary distorted state (D) at $\rho = 0.8$ (•); periodic oscillating state (O) at $\rho = 0.91$ (curve 1); periodic rotating state PR_1 slightly above the gluing bifurcation at $\rho = 0.917$ (curve 2); periodic rotating state PR_2 at $\rho = 0.95$ (curve 3). (c) $\chi = 0.74$: stationary distorted state (D) at $\rho = 0.99$ (•); periodic oscillating state (O) at $\rho = 0.9925$ (curve 1); periodic rotating state PR_1 slightly above the gluing bifurcation at $\rho = 0.9932$ (curve 2); periodic rotating state PR_2 slightly above the saddle-node bifurcation at $\rho = 0.9936$ (curve 3, dashed line); quasi-periodic rotating state at $\rho = 1.5$ (curve 4).

4. Transverse effects

4.1. The role of finite beamsize

As mentioned in Section 2.3.2, most theoretical works treating light-induced director reorientation in nematics use the plane wave approximation, where not only the incident light, but all physical variables are assumed to be dependent only on the z coordinate. An exception to this is the investigation of the primary instability (the OFT) in various geometries, where the role of the finite transversal intensity profile of the light has been investigated [62–65]. As it was readily noted, the transverse reorientation profile of the nematic is able to follow the decrease of the laser beam size only to a certain point. Elasticity prevents the reorientation profile from being too sharp, even if the laser spotsize is very small. Thus, as the spotsize is decreased, the width of the reorientation profile tends to a finite value, the nematic reorients outside the illuminated area as well. Correspondingly, the intensity required to induce the transition grows, because a narrow region of light-induced torque must keep balance with the elastic torques of a more extended region of director distortion. This effect is sometimes termed the transverse non-locality of nematics. The mathematical difficulties of

including the transversal coordinates were already evident in these first studies. Instead of the 1 + 1D PDEs that we have to start with in the plane wave theory, we are confronted with a full 3 + 1D PDE problem.

In the context of light-induced dynamical behaviour, investigations on the effects of finite beamsize have not been performed until very recently. This is at first surprising, as experiments in this field have always been performed with "narrow" beams, whose transverse size was the same order of magnitude as the cell thickness, and not with "wide" beams, whose transverse size would be much larger. Besides the mathematical difficulties, this situation was no doubt due to the fact that considerable progress has been made in understanding these phenomena using the plane wave theory, so transverse effects appeared to be of less importance.

A novel approach was adopted recently in a series of experiments, where the influence of the finite beam size on the dynamical behaviour of a nematic has been investigated systematically. These studies uncovered a lot of interesting phenomena and the need for a proper theory describing finite beamsize effects became evident. The studies also proved however, that finite beamsize effects are not of decisive importance until at least one transverse dimension of the laser beam is significantly smaller than the cell thickness.

4.1.1. Circular beam profile

One series of studies investigated the well known director precession phenomena induced by perpendicularly incident, circularly polarised light [18,66,67] (see also Section 3.2). In these studies, the ratio of the Gaussian beam width to the cell thickness $\delta = w_0/L$ was a new control parameter, in addition to the normalised intensity of the incident light. In particular, the series of bifurcations were investigated at several values of δ as the light intensity was increased. It was found, that when the beam width is significantly smaller than the cell thickness (at $\delta = 0.37$ in [18]), new dynamical regimes can be seen, among them even some stochastic ones, which is unusual for this geometry. (The nature of these regimes however, was not identified clearly.) The reason for this change of dynamics was also not clear in these works, but several possible causes have been speculated on. One idea, was that the so-called walk-off is to blame, i.e. the relative displacement of the ordinary and extraordinary beams during propagation within the liquid crystal medium. This question was investigated further in a theoretical model [66]. The theory, which included δ as a control parameter, used some fairly artificial assumptions, for example the incident intensity was assumed to be a step-function in the transverse plane, and director reorientation was assumed to be dependent only on z. Nevertheless, a critical value for δ was found (about 0.2–0.3 depending on L), bellow which the bifurcation diagram changes compared to the plane wave case. However, the model never recovered the secondary Hopf bifurcation that leads to the NUP regime, so in the limit of large δ (the true plane wave case) it does not yield the correct bifurcation diagram. Therefore, while one cannot exclude that walk-off can be important in some situations, no real dynamical models support this idea reliably at the moment.

In another work, a simple model has been devised using coupled rotators that are driven by the light [67]. While admittedly a toy model, it did reveal an interesting result, namely that if $\delta > 0.7$, the rotators are all synchronised, i.e. the behaviour of the system is exactly the same as for the infinite plane wave case. On the other hand, this toy model neglected effects such as the twist deformations of the director, which are known to be important in this geometry for the description of the secondary instability (the Hopf bifurcation to the NUP regime, see Section 3.2.2).

4.1.2. Elliptical beam profile

Another set of studies investigated the OFT in geometries where the laser beam was incident perpendicularly upon the nematic cell and the transverse profile of the beam was made highly elliptical. The intensity distribution could thus be characterised by two width parameters w_x and w_y, corresponding to the beam waist size in the directions of the major and minor axis of the intensity profile ellipse. While one was always the same order of magnitude as the cell thickness, the other was usually about ten times smaller than the larger one ($w_x = 100\,\mu\text{m}$, $w_y = 10\,\mu\text{m}$ were typical values). For linearly polarised light, there is an additional control parameter that can be changed easily, the angle β between the direction of the incident polarisation and the direction of the major axis of the intensity distribution ellipse. The two width parameters w_x and w_y were not really control parameters, as they cannot be changed easily in the experiment. Nevertheless, the profile ellipticity $\mu = w_x/w_y \sim 10$ was noted and may well prove essential for characterising the interaction.

Observations in this geometry revealed interesting dynamical regimes. Using linearly polarised light, oscillatory behaviour was found above a secondary bifurcation in [68]. The oscillations were initially regular, then became more

irregular as the intensity was increased. Similar observations were published in [69], and clear experimental evidence of on–off intermittency in the director rotation was also found for a similar setup using circularly polarised light [17].

The first qualitative theoretical explanations of these phenomena were published along with the observations. They were probably inspired by the appealingly simple explanation of self-induced stimulated light scattering in terms of photon spin deposition in the nematic (see Section 3.2). They showed [68–70], that beam shape ellipticity is, in itself, a source of an additional torque on the director. This torque is absent for circularly symmetric beams, and can be attributed to the transfer of orbital angular momentum from the light to the nematic. Furthermore, this torque is present for elliptically shaped laser beams even if the light is unpolarised, and also if the light carries, on the average, zero orbital angular momentum. The important ingredient was found to be the breaking of the azimuthal symmetry. These works thus suggested that the complex behaviour observed was due to some sort of competition between spin and orbital angular momentum transfer. They were however, rather qualitative arguments.

The first attempt to derive a "simple" working model from the basic equations that could account for the complex dynamical behaviour, arrived at a set of nonlinear ODEs for six scalar variables that describe the director orientation dynamics [71] when light is polarised linearly. It used a fairly restrictive family of functions to describe the director orientation. A single polar angle amplitude θ_0 was used for the magnitude of the reorientation, whose x–y dependence was assumed to be elliptical in shape, with a Gaussian cross-section having two independent width parameters θ_1 and θ_2. The angle γ between the major axis of the reorientation ellipse and that of the intensity ellipse was also a dynamical variable. The azimuthal orientation was described by two variables, the average orientation ϕ_0 and the twist amplitude ϕ_1. The azimuthal orientation was thus assumed to be homogeneous in the cell plane. Clearly, this set of variables constitutes one of the simplest possible models (which shows the mathematical difficulty that is encountered in this problem).

The study neglected flow, used the GOA for the light propagation problem, and also neglected the distortion of the intensity ellipse (thus excluding the spatial displacement of the ordinary and extraordinary beams i.e. walk-off from the model). It also assumed reorientation to be small and used a power series expansion with respect to θ_0, but the phase shift between ordinary and extraordinary light was calculated exactly. The most interesting property of this study was, that it explicitly expressed the interaction terms that are due to light spin change and to light orbital angular momentum change in the director equations. The calculations (and the corresponding experiments) were done with a highly distorted beam: $L = 50\,\mu\text{m}$, $w_1 = 178\,\mu\text{m}$, $w_2 = 12\,\mu\text{m}$, i.e. $\mu = w_x/w_y = 15$!

The results of this model were intriguing. It predicted multistability above the OFT threshold, at points where a balance is achieved between the spin and the orbital angular momentum deposition. The experimental results in parameter space were somewhat "coarse" for a complete verification of this prediction, but the agreement between theory and measurement was notable. The model also reproduced the regular oscillatory behaviour of the director above a certain light intensity, but irregular or chaotic oscillations observed in certain regions of the intensity and β were not found. It was also noted, that without the inclusion of director twist ϕ_1 even the regular oscillations were not reproduced. Interestingly enough, oscillations in the model were also absent if the one constant approximation was utilised in the description of the elastic energy of the nematic.

The above model was generalised slightly to treat circularly polarised light [72]. This time, oscillating and rotating states were found in the model, and a gluing bifurcation was identified to take place between them. The experiment published alongside does not contradict this, but is not decisive enough to confirm the suggested scenario either. The on–off intermittency observed however, (and also found in [17]) was not predicted by the model, suggesting that it is, after all, slightly oversimplified to encompass the dynamics of the strongly nonlinear domain.

4.1.3. Questions on finite beamsize effects

It is difficult to present a clear picture in the case of finite beamsize effects, the problems they pose seem to be mostly open. It is clear, that a comprehensive theory is still missing, that existing models are too oversimplified to grasp every essential detail and reproduce the complex dynamical behaviour seen in the experiments. The fact that one model neglects certain features of the interaction (e.g. walk-off or twist deformations), that the other model shows to be of decisive importance, adds to the confusion. It is also quite possible, that different features of the interaction become important in different geometries. It is, however quite remarkable, that whatever the geometry, at least one transverse size of the beam must be significantly smaller than the cell thickness ($w < L/2$). Without this, no novel dynamical regimes have been seen.

4.2. Transverse pattern formation

It was already mentioned in the introductory sections, that the plane wave approximation used in the description of light-induced dynamics in nematics is more appropriately called the 1D approximation, as all physical variables are assumed to depend only on z. It is well known from the theory of extended nonlinear systems however, that a spatially homogeneous state may loose stability to a finite wavelength perturbation, leading to pattern formation. Then the dependence of the physical variables in the transverse plane develops spontaneously. Thus even if the light illuminating the cell is truly an infinite plane wave, spontaneous pattern formation may take place. (In the course of any linear stability analysis that investigates the stability of some stationary state, one considers spatially periodic perturbations. The wave vector $\vec{k}$ of the mode whose time exponent becomes positive first as some control parameter is varied, is called the critical wave vector $\vec{k}_c$. If this is zero, i.e. the critical wavelength is infinite, the bifurcation is said to be spatially homogeneous. If $\vec{k}_c \neq 0$, i.e. the critical wavelength is finite, it is said to be spatially inhomogeneous.)

There are several indications that instabilities, which spontaneously break the transverse symmetry are to be expected in the case of light induced dynamics in nematics. On the one hand, periodic patterns are known to develop in the static (low frequency) electric field or magnetic field induced Fréedericksz transition if the elastic constants are sufficiently different [73,74]. On the other hand, homoclinic bifurcations, which occur in several geometries in light induced director dynamics, are known to generate spatial instabilities. In fact any, almost homoclinic cycle is generically unstable in a spatiotemporal instability, which is either a phase instability, or a finite wavelength period doubling instability [75]. Thus very complicated behaviour (probably spatio-temporal chaos) is expected to occur in the vicinity of these homoclinic bifurcations, if we consider a truly infinite plane wave illumination, but allow transversal spatial dependence. Despite this, there are few theoretical papers that treat this subject. The reasons are that on the one hand, exploring the precise nonlinear behaviour in the spatially extended case is prohibitively difficult, and on the other, that there are no experimental works that even come close to realising the plane wave limit, so there are no observations to contrast with theory.

Despite the difficulties, a limited amount of effort did go into exploring transverse pattern formation. In [19], the simple models of director dynamics in two geometries were generalised by adding a slow x–y dependence of the mode amplitudes, and exploring the effects. In the case of a linearly polarised, obliquely incident light, it was noted that the primary bifurcation (the OFT) is always a homogeneous bifurcation (i.e. $\vec{k}_c = 0$), both when it is a pitchfork bifurcation (line 1 in Fig. 4) and when it is a Hopf one (line 2 in Fig. 4). In this second regime, a weakly nonlinear analysis was also performed, and the coefficients of the relevant complex Ginzburg–Landau equations were derived [77]. The linear dispersion parameter turned out to be zero, and the nonlinear dispersion parameter was in a regime where stable plane wave and spiral solutions are possible [76]. The linear stability of the stationary distorted state above the primary pitchfork bifurcation was also re-examined in the vicinity of the secondary Hopf-bifurcation. It was shown, that this bifurcation is homogeneous only if all the elastic constants are equal $K_1 = K_2 = K_3$. This is a novelty compared to the magnetic [73], and the electric [74] field induced Fréedericksz transition, where there is a lower limit to K_1/K_2 and K_1/K_3 bellow which $\vec{k}_c = 0$.

The spatially extended version of the simple model in the oblique incidence geometry [19] was also used to investigate nonlinear behaviour of the system as it neared the first gluing bifurcation (still within the range of validity of the simple model). As foreseen, before reaching the gluing bifurcation, the system reaches a turbulent state [78]. Surprisingly, this was found to be generated by so-called retracting fronts [79], which suppress perturbations in the vicinity of an unstable state.

The linear stability of the stationary distorted state in the linearly polarised, obliquely incident geometry was also analysed more precisely using numerical methods [20]. This time not pure, but dye-doped nematics were considered. The reason was, that for pure nematics, one needs a very large laser to induce the OFT and the dynamical behaviour above it over a substantial area of the cell, as the required intensities are large. On the other hand, similar effects have been observed in dye-doped nematics, where the required intensity can be over two orders of magnitude smaller. As dyes have non-negligible absorption, this also had to be taken into account. While the equations become more cumbersome, including absorption finally leads only to some quantitative changes, namely raises bifurcation thresholds by a few percent. In the analysis, the exact reorientation profiles were calculated first, then their stability was investigated with respect to spatially periodic perturbations (proportional to $\exp[\mathrm{i}(qx + py)]$). The neutral surface was calculated and its minimum, the first mode that destabilises the stationary state was found. (The neutral surface is defined as the values of the intensity $\rho(p, q)$ where the real part of the time exponent belonging to a perturbation with wavenumber (p, q)

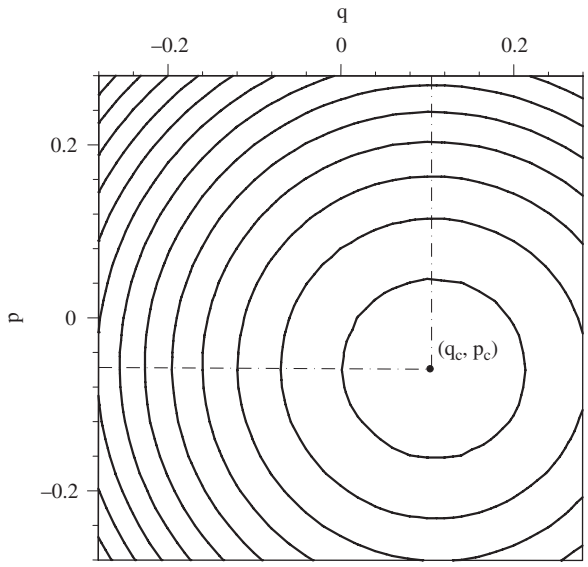

Fig. 10. Contour plot of the neutral surface as a function of the wave vector components p and q calquated for $\alpha = 11°$. (p and q are measured in units of $1/L$.) The minimum of the surface yields the critical wave vector components $q_c = 0.11/L$ and $p_c = -0.06/L$.

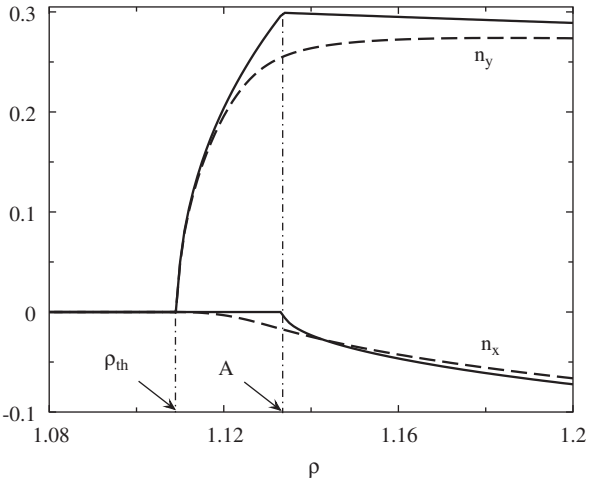

Fig. 11. Profiles of the director components n_x, n_y versus ρ at some z inside the layer (not at the middle). Solid and dashed lines correspond to $\alpha = 0°$ and $0.5°$, respectively. ρ_{th} is the threshold intensity of the OFT, calculated for a nematic doped with dye. It is greater than unity because of light absorption (see [20] for details). Point A is a pitchfork bifurcation to a stationary state with broken x-reflection symmetry ($\alpha = 0°$).

vanishes.) An example of the neutral surface plot is shown in Fig. 10. As for the previous study, a finite wavelength instability was found for the generic case, $\vec{k}_c$ was zero only if the elastic constants were equal. Since this secondary bifurcation is a Hopf-instability, one thus expects to see travelling waves above threshold.

The results obtained confirmed that the bifurcation is always inhomogeneous unless the elastic constants are all equal. The magnitude of the critical wave vector was also calculated as a function of the ratios K_1/K_3 and K_2/K_3, which characterise the elastic anisotropy. It was found that as the anisotropy increases (i.e. as the ratios decrease), the magnitude of the critical wavevector also increases. For the materials typically used in the experiments investigating light-induced director dynamics, the order of magnitude for $|\vec{k}_c| \sim 0.1/L$. This means that to observe pattern formation, the laser beam spotsize should be about 100 times wider than the cell thickness!

Besides uncovering novel phenomena, these studies were very useful in marking the upper limit of the laser spot size, where the plane wave (or 1D) approximation may be used to model director dynamics. Clearly, if the spot size is about $w_0 \leqslant 10L$, the dependence of the physical quantities on the transversal coordinate will be suppressed, and the plane wave approximation will be valid.

Another interesting result also came to light, when the general analysis [20,55] allowing x–y dependence of the reorientation was used to investigate the perpendicular incidence ($\alpha = 0$) limit. This is the geometry of the classical OFT induced by linearly polarised light, which has always been analysed by assuming that the director reorientation remains in the plane spanned by the original homeotropic orientation and the direction of polarisation (the y–z plane). Although in the $\alpha = 0$ case, the external symmetry breaking in the x direction vanishes, so the reorientation is initially really along the y direction, it turned out that the OFT is shortly followed by another stationary instability. This spontaneously breaks the reflection symmetry with respect to x and precedes the secondary Hopf bifurcation. It is shown by point A in Fig. 11. It is also seen from this figure, that the secondary pitchfork bifurcation is destroyed in the case of oblique incidence, which can be interpreted as an imperfect bifurcation with respect to the angle α [55,56].

5. Various generalisations

As mentioned in the introduction, nematics driven by intensive light are an excellent playground for observing various nonlinear phenomena, because the experimental realisation is fairly simple and inexpensive. It is also easy to generalise the simple system by including various static fields, adding further light fields, or modulating the light intensity in time. This allows the study of various topics in nonlinear dynamics such as periodic forcing, chaos control, and more. The range of possibilities is very wide, this section contains just a few examples that have been investigated.

5.1. Cholesteric nematic mixtures

One such example is the study of cholesteric-nematic mixtures with initial homeotropic orientation in the field of circularly polarised light. These mixtures are obtained by doping a nematic liquid crystal with chiral molecules (a cholesteric liquid crystal) that can induce a helix structure of the director profile [6]. This helical structure is characterised by a pitch p (or a wavevector $q = 2\pi/p$) that can be either positive or negative, distinguishing between right- and left-handed helices. It is worth noting that these mixtures have been widely used in the realisation of twisted cells for liquid crystal displays that are usually made in planar geometry. For this reason, only a few studies were devoted to the case of homeotropic alignment which is nevertheless interesting because of the incompatibility between a bulk homeotropic alignment and the helix formation. In fact, the bulk homeotropic orientation is stable for small values of $|q|$ while it is unstable above a threshold value, q^*, where a helix structure is formed. In spatially extended systems this leads to the formation of twisted domains, which can be eventually quenched by applying a suitable electric field [80,81].

The theory for cholesteric–nematic mixtures is the straightforward extension of the theory for pure nematics described in the previous sections. To generalise to a chiral nematic case, one has to add a chiral part to the elastic free energy density $F_{\mathrm{chol}}^{(\mathrm{elastic})} = F^{(\mathrm{elastic})} + qK_2(\mathbf{n}\cdot\boldsymbol{\nabla}\times\mathbf{n})$, where $F^{(\mathrm{elastic})}$ is given by Eq. (3). Then, the intrinsic helical structure induced by the chiral dopant is taken into account by writing the twist angle Φ as $\Phi_{\mathrm{chol}}(z,t) = \Phi(z,t) + k_2 qz$, where $k_2 = K_2/K_3$ and $\Phi(z,t)$ is the twist angle for a pure nematic introduced in Section 3.2.1.

In [82–84] the reorientation of the director induced by linearly and/or circularly polarised light impinging at normal incidence onto a cholesteric–nematic sample with homeotropic anchoring conditions has been studied. It was shown, that the initial homeotropic alignment is unstable above a threshold value, I_{th}, which is a function of q and is smaller than for the $q = 0$ case. For CP light the expression for the threshold is given by $\rho_{\mathrm{th}} = 1 - \widetilde{q}^2 k_2^2$ [84], where $\widetilde{q} = qL/\pi$. For LP light, ρ_{th} was shown to satisfy the transcendent equation $\rho_{\mathrm{th}} = (4k_2^2\widetilde{q}^2/\pi\delta)\cdot\tan(\pi\delta/2)$, where $\delta = \sqrt{2(\rho_{\mathrm{th}} + 2k_2\widetilde{q}^2)}$ [83]. As is seen, q enters quadratically in the above expressions, i.e. the decrease of the OFT threshold is insensitive to the sign of q, as expected. The nature of the OFT and the director reorientation was demonstrated to depend significantly on the relative helicity of the light field and the chiral mixture. Denoting by CP^+ [CP^-] the case of a circular polarisation with same [opposite] helicity to the one of the material and by LP the case of linearly polarised excitation, one can mention for instance the two following points: (i) a large optical bistability observed for LP light when $|q|$ is large enough and (ii) the reorientation for CP^- is similar to the one of LP light with $q = 0$.

In [82] the numerical solution for LP light near the OFT for different values of q was found. It was shown, that the OFT might be of first-order with hysteresis, even when for zero doping it is of second order. In [83] an approximate solution for the director components near the OFT under the assumption of small distortion was derived. In [84] the authors extended the model beyond the small distortion region by numerically integrating the torque equations both for stationary (LP light) and for time dependent (CP light) cases. In particular, the model confirmed the birefringence freezing effect [83] which refers to the fact that the optically induced phase delay between ordinary and extraordinary waves remains about π over a relatively wide range of intensities above the OFT. However, it was unable to reproduce other experimental observations [84] like the secondary transition to a largely distorted state or the bistability loop.

In [85], a detailed theoretical study of the optical reorientation induced by CP light in chirally doped nematics has been done. The competition between an *intrinsic* helical pattern (owing to the chiral dopant) and an *extrinsic* helical pattern (owing to the light) was shown to be at the origin of the complex behaviour. This mechanism might be described as follows. Angular momentum deposited into the sample when light propagates through it leads to a twist distortion, which can be called a light induced spiral. This spiral can be of the same or opposite helicity as the one induced by the chiral dopant. In the latter case this might lead to an unwinding of the intrinsic helical structure. It should be noted, that here we discuss those values of q which are lower than the critical value $\widetilde{q}^* = 1/k_2$ for CP light. (Above this value the homeotropic alignment is destabilised in favour of a twisted structure already without light.) In the calculations of [85] $\widetilde{q}^*$ turns out to be 2.74 that corresponds to the critical pitch of the spiral $p^* = 0.73L$ i.e. it is of the order of the thickness of the layer.

An approximate model, which is capable of describing the state of uniform director precession (the UP state, see Section 3.2.2) and is the straightforward generalisation of the approximate model developed in [45] (see Section 3.2.1), has been proposed in [85]. The OFT was found to be continuous if $\widetilde{q} < \widetilde{q}_c$ and discontinuous in the opposite case. The value of $\widetilde{q}_c$ turned out to be small and was found to be $\widetilde{q}_c \sim 5.8 \times 10^{-3}$ in [85]. In addition, optical bistability was predicted in the vicinity of the continuous OFT for small values of $|\widetilde{q}|$.

Then the full numerical study was also performed in [85] which yielded the whole bifurcation scenario taking place for right- and left-handed circular polarisations. The bifurcations that have been previously observed for CP light were recovered. In particular, the nature of the bifurcation to a large reoriented state, the intermediate dynamical regimes and instabilities experienced by the system were demonstrated to depend strongly on q, as is shown in Fig. 12. Note that Fig. 12(c) corresponds to the case of a pure nematic and coincides with Fig. 5 from Section 3.2.2. Interestingly, nutation-precession states (NUP states) introduced in Section 3.2.2 exist only in a finite window of the chiral parameter $\widetilde{q}_1 < \widetilde{q} < \widetilde{q}_2$, where $\widetilde{q}_1 \simeq -1.17$ and $\widetilde{q}_2 \simeq 0.53$. Two typical examples are shown in Fig. 12(b),(c). It should be noted that inside this window there are one or more intervals of ρ where the NUP states exist. We refer the interested reader to [85] for further details. The bifurcation scenarios outside this window are shown in Fig. 12(a),(d). As one sees from Fig. 12(a), where $\widetilde{q} = -1.235$, the birefringence freezing effect takes place approximately for $1.25 < \rho < 2.0$. On the contrary, for $\widetilde{q} > \widetilde{q}_2$, it does not occur as illustrated by Fig. 12(d) where $\widetilde{q} = 0.7$. If one starts from the UP state above the OFT and the intensity ρ is increased, a discontinuous transition to a largely reoriented state with hysteresis takes place in both cases, but for $\widetilde{q} < \widetilde{q}_1$ the hysteresis loop is much wider. In fact, these results describe qualitatively the observations reported in [84] both for the CP^+ and CP^- geometries.

In [85] only qualitative agreement between theory and experiment was found. For instance, the numerical values of the bifurcation thresholds turned out to be quite different. The reason for that could be, as before, due to the use of a finite beam size in the experiment whereas the theory assumed an infinite plane wave.

5.2. Chaos control

Another example of a slightly more general system is one where an additional laser beam also traverses the nematic, in addition to the primary beam that induces nonlinear dynamics. This beam can be weak compared to the first one, yet if its field does exert some torque on the molecules, the effect on the dynamical scenario can be considerable. It has been shown in [89], that the chaotic behaviour induced by linearly polarised, obliquely incident light can be controlled effectively using an additional beam of orthogonal linear polarisation, whose intensity may be as low as 10–100 times smaller than that of the primary laser beam. This additional beam can stop periodic oscillations, stabilise periodic orbits within the chaotic regime or induce whole new dynamical behaviour, depending on the intensity of the primary beam. The simple models derived for this geometry were generalised to include this second beam [90]. The processes of orbit stabilisation and the novel dynamical regimes were then studied in detail using the generalised model.

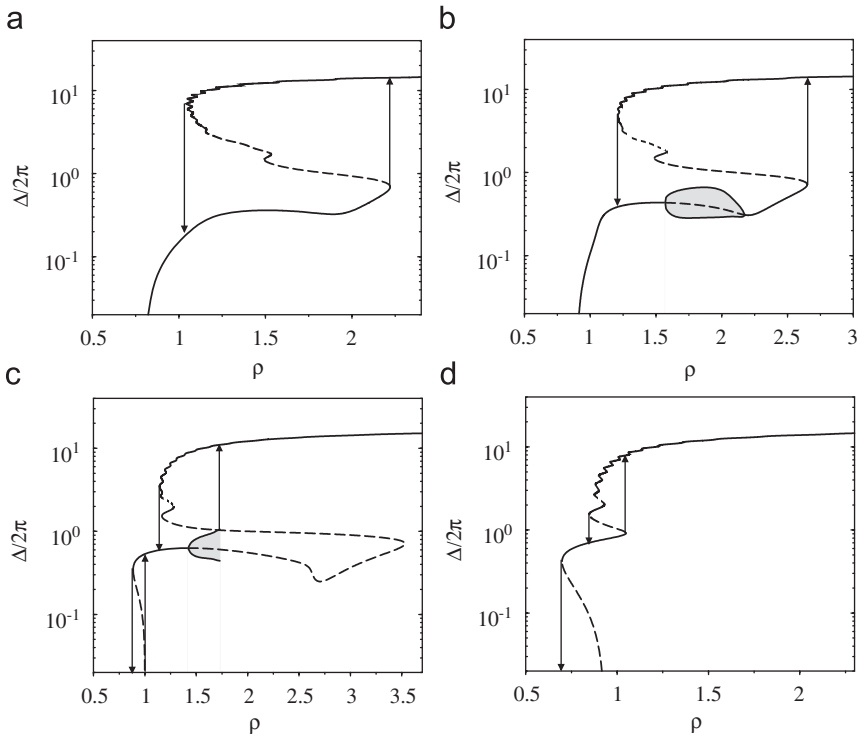

Fig. 12. Bifurcation diagram of a cholesteric–nematic mixture distorted by CP light, showing the phase delay $\Delta/2\pi$ versus normalised intensity ρ for different wavevectors $\widetilde{q}$. The lines mark the reorientation amplitude of various limit-cycle solutions. (a) $\widetilde{q} = -1.235$, (b) $\widetilde{q} = -0.9$, (c) $\widetilde{q} = 0$ and (d) $\widetilde{q} = 0.7$. The solid (dashed) lines are stable (unstable) states and the gray regions refer to precession–nutation regimes.

5.3. Periodic forcing

Another interesting direction of study is examining the response of a nematic driven by light with a periodically modulated intensity near a Hopf bifurcation [86]. As was described in Section 3.2, for a constant intensity CP light the OFT leads to a regime where the director precesses uniformly (UP1 regime), and this state looses stability in a Hopf bifurcation, which leads to a quasiperiodic regime of director precession–nutation (NUP regime). In a coordinate system rotating with the precession frequency f_0, the mode amplitudes acquire a time dependence at this bifurcation, with a new frequency f_1 appearing associated with the nutation. In the geometry with obliquely incident, linearly polarised light (see Section 3.1) the system settles to a stationary distorted state (fixed point) above the OFT (for angles of incidence not too far from perpendicular). A further increase of the intensity leads to a secondary supercritical Hopf bifurcation. The response of the system to a periodic modulation of the intensity with frequency f and amplitude $\mathrm{d}\rho$, depends on whether the ratio f/f_1 will be a rational or an irrational number and is expected to have an Arnold's tongue structure in the $(f_1/f, \mathrm{d}\rho)$ plane [87,88]. In [86] one particular tongue $f_1/f = 2/1$ was reconstructed for both cases by simulating the system of ODEs for the mode amplitudes. It was found both theoretically and experimentally that outside this tongue, the response of the system is quasiperiodic for small forcing amplitudes $\mathrm{d}\rho$. For moderate to large forcing amplitudes, a lot of different interesting phenomena occurred, among which the route to chaos through a cascade of period doubling bifurcations and windows of regular behavior inside the chaotic region were found. Fortunately the tongue, as well as the region of period-doubling bifurcations followed by a chaotic region turned out to be wide in the $(f_1/f, \mathrm{d}\rho)$ plane, so an experimental observation turned out to be possible.

6. Summary and outlook

In this paper, we have presented an overview of recent advances in understanding the complex nonlinear phenomena that arise when a cell of nematic liquid crystal is irradiated by strong laser light. Interesting nonlinear dynamics

have been observed in this system for light intensities above the optically induced Fréedericksz transition threshold, for several geometries (linearly polarised light with oblique incidence, circularly and elliptically polarised light with perpendicular incidence). Our focus was on the recent progress made in modelling and understanding these dynamical phenomena. We have listed the various approximations that can be used in solving the set of equations that describe the system—the nematodynamical equations for the liquid crystal, coupled to Maxwell's equations for the propagation of light. We have summarised the most important results obtained from various theoretical calculations, and contrasted the dynamical regimes of the calculations with those observed in the experiments. These comparisons yield valuable insight as to which features of the interaction are important to consider in a theory. In a few cases, surprisingly simple models are successful in recovering a considerable part of the bifurcation scenario. In other cases, this is not so, and only an extensive numerical calculation is able to produce results that are in agreement with observations. In some cases, even the flow of the nematic (which is almost always neglected in theories) can be shown to play a considerable part in shaping the dynamical landscape. Another major complication is the use of very narrow beams, which yields new, interesting and largely unexplained results.

As probably evident from the previous sections, light induced dynamical phenomena in nematics are extremely diverse, and still present a large number of open problems to solve. The most interesting problems on the side of fundamental research at the moment seem to be associated with finite beamsize effects. This is an area where a number of recent observations still await proper explanation, while new experiments are being performed. On the other hand, phenomena in this field seem to be finding their way to technological applications. One example is the construction of all-optical photonic switching devices using nematics [91], and more will probably follow soon.

Acknowledgements

This paper is a tribute to the memory of Professor Lorenz Kramer, with whom we have had the privilege and pleasure of working on this exciting field before his sudden death over a year ago. His inspiring and energetic person will be greatly missed by us and many others.

We are very grateful to Professor Ágnes Buka for supplying us with numerous valuable comments while writing the manuscript.

References

[1] N.V. Tabiryan, A.V. Sukhov, B.Ya. Zel'dovich, Mol. Cryst. Liq. Cryst. 136 (1985) 1–140.
[2] I.C. Khoo, Liquid Crystals: Physical Properties and Nonlinear Optical Phenomena, Wiley Interscience, New York, 1994.
[3] I.C. Khoo, S.T. Wu, Optics and Nonlinear Optics of Liquid Crystals, World Scientific, Singapore, 1993.
[4] F. Simoni, Nonlinear Optical Properties of Liquid Crystals and Polymer Dispersed Liquid Crystals, World Scientific, Singapore, 1997.
[5] F. Simoni, O. Francescangeli, J. Phys.: Condens. Matter 11 (1999) R439.
[6] P.G. de Gennes, J. Prost, The Physics of Liquid Crystals, Clarendon Press, Oxford, 1993.
[7] S. Chandrasekhar, Liquid Crystals, Cambridge University Press, Cambridge, 1994.
[8] F.M. Leslie, Quart. J. Mech. Appl. Math. 19 (1966) 357.
[9] O. Parodi, J. Phys. (Paris) 31 (1970) 581.
[10] L. Marrucci, G. Abbate, S. Ferraiuolo, P. Maddalena, E. Santamato, Mol. Cryst. Liq. Cryst. 237 (1993) 39.
[11] D.O. Krimer, G. Demeter, L. Kramer, Phys. Rev. E 71 (2005) 051711.
[12] G. Demeter, D.O. Krimer, L. Kramer, Phys. Rev. E 72 (2005) 051712.
[13] D.W. Berreman, J. Appl. Phys. 46 (1975) 3746.
[14] C.Z. van Doorn, J. Appl. Phys. 46 (1975) 3738.
[15] S.A. Jewell, J.R. Sambles, Appl. Phys. Lett. 82 (2003) 3156.
[16] S.A. Jewell, J.R. Sambles, Appl. Phys. Lett. 84 (2004) 46.
[17] A. Vella, A. Setaro, B. Piccirillo, E. Santamato, Phys. Rev. E 67 (2003) 051704.
[18] E. Brasselet, B. Doyon, T.V. Galstian, L.J. Dube, Phys. Rev. E 69 (2004) 021701.
[19] G. Demeter, L. Kramer, Mol. Cryst. Liq. Cryst. 366 (2001) 2659.
[20] D.O. Krimer, G. Demeter, L. Kramer, Phys. Rev. E 66 (2002) 031707.
[21] E. Santamato, Y.R. Shen, J. Opt. Soc. Am. A 4 (1987) 356.
[22] D.W. Berreman, J. Opt. Soc. Am. 62 (1972) 502.
[23] B.Ya. Zel'dovich, S.K. Merzlikin, N.F. Pilipetskii, A.V. Sukhov, N.V. Tabiryan, JETP Lett. 37 (1983) 677.
[24] A.S. Zolot'ko, V.F. Kitaeva, N. Kroo, N.N. Sobolev, A.P. Sukhorukov, V.A. Troshkin, L. Csillag, Sov. Phys. JETP 60 (1984) 488.
[25] V.F. Kitaeva, N. Kroo, N.N. Sobolev, A.P. Sukhorukov, V.Yu. Fedorovich, L. Csillag, Sov. Phys. JETP 62 (1985) 520.
[26] A.S. Zolotko, V.F. Kitaeva, N.N. Sobolev, V.Yu. Fedorovich, A.P. Sukhorukov, N. Kroo, L. Csillag, Liq. Cryst. 15 (1993) 787.

[27] G. Cipparrone, V. Carbone, C. Versace, C. Umeton, R. Bartolino, F. Simoni, Phys. Rev. E 47 (1993) 3741.
[28] V. Carbone, G. Cipparrone, C. Versace, C. Umeton, R. Bartolino, Mol. Cryst. Liq. Cryst. Sci. Technol. Sect. A 251 (1994) 167.
[29] V. Carbone, G. Cipparrone, C. Versace, C. Umeton, R. Bartolino, Phys. Rev. E 54 (1996) 6948.
[30] C. Versace, V. Carbone, G. Cipparrone, C. Umeton, R. Bartolino, Mol. Cryst. Liq. Cryst. Sci. Technol. Sect. A 290 (1996) 267.
[31] E. Santamato, P. Maddalena, L. Marrucci, B. Piccirillo, Liq. Cryst. 25 (1998) 357.
[32] N.V. Tabiryan, A.L. Tabiryan-Murazyan, V. Carbone, G. Cipparrone, C. Umeton, C. Versace, Optics Commun. 154 (1998) 70.
[33] G. Demeter, L. Kramer, Phys. Rev. Lett. 83 (1999) 4744.
[34] G. Demeter, Phys. Rev. E 61 (2000) 6678.
[35] A. Arneodo, P. Coullet, C. Tresser, Phys. Lett. 81A (1981) 197.
[36] Y. Kuramoto, S. Koga, Phys. Lett. 92A (1982) 1.
[37] D.V. Lyubimov, M.A. Zaks, Physica D 9 (1983) 52.
[38] G. Russo, V. Carbone, G. Cipparrone, Phys. Rev. E 62 (2000) 5036.
[39] V. Carbone, G. Cipparrone, G. Russo, Phys. Rev. E 63 (2001) 051701.
[40] G. Demeter, L. Kramer, Phys. Rev. E 64 (2001) 020701.
[41] G. Demeter, L. Kramer, Mol. Cryst. Liq. Cryst. 375 (2002) 745.
[42] E. Brasselet, Phys. Rev. E 72 (2005) 013701.
[43] E. Santamato, B. Daino, M. Romagnoli, M. Settembre, Y.R. Shen, Phys. Rev. Lett. 57 (1986) 2423.
[44] E. Santamato, M. Romagnoli, M. Settembre, B. Daino, Y.R. Shen, Phys. Rev. Lett. 61 (1988) 113.
[45] L. Marrucci, G. Abbate, S. Ferraiuolo, P. Maddalena, E. Santamato, Phys. Rev. A 46 (1992) 4859.
[46] A. Hertrich, W. Decker, W. Pesch, L. Kramer, J. Phys. II France 2 (1992) 1915.
[47] A.G. Rossberg, A. Hertrich, L. Kramer, W. Pesch, Phys. Rev. Lett. 76 (1996) 4729.
[48] A.S. Zolot'ko, A.P. Sukhorukov, Sov. Phys. JETP Lett. 52 (1990) 62.
[49] S.D. Durbin, S.M. Arakelian, Y.R. Shen, Opt. Lett. 6 (1981) 411.
[50] E. Brasselet, B. Doyon, T.V. Galstian, L.J. Dube, Phys. Lett. A 299 (2002) 212.
[51] E. Brasselet, B. Doyon, T.V. Galstian, L.J. Dube, Phys. Rev. E 67 (2003) 031706.
[52] D.O. Krimer, G. Demeter, L. Kramer, Mol. Cryst. Liq. Cryst. 421 (2004) 117.
[53] E. Brasselet, T.V. Galstian, L.J. Dube, D.O. Krimer, L. Kramer, J. Opt. Soc. Am. B 22 (2005) 1671.
[54] H.L. Ong, Phys. Rev. A 28 (1983) 2393.
[55] D.O. Krimer, Ph.D. Thesis, University of Bayreuth (2004). URL: http://opus.ub.uni-bayreuth.de/volltexte/2004/98/
[56] D.O. Krimer, G. Demeter, L. Kramer, Dynamical phenomena in nematic liquid crystals induced by light in Self-Assembly Pattern Formation and Growth Phenomena, in: A. Golovin, A. Nepomnyashchy (Eds.), Nano-Systems, NATO Science Series II, vol. 218, Springer, Berlin, 2006, pp. 83–122.
[57] P. Glendinning, Stability, Instability and Chaos, Cambridge University Press, Cambridge, 1996.
[58] B.Y. Zel'dovich, N. Tabiryan, Sov. Phys. JETP 55 (1982) 656.
[59] E. Santamato, G. Abbate, P. Maddalena, L. Marrucci, Y.R. Shen, Phys. Rev. Lett. 64 (1990) 1377.
[60] A. Vella, B. Piccirillo, E. Santamato, Phys. Rev. E 65 (2002) 031706.
[61] D.O. Krimer, L. Kramer, E. Brasselet, T.V. Galstian, L.J. Dube, J. Opt. Soc. Am. B 22 (2005) 1681.
[62] L. Csillag, J. Janossy, V.F. Kitaeva, N. Kroo, N.N. Sobolev, Mol. Cryst. Liq. Cryst. 84 (1982) 125.
[63] E. Santamato, Y.R. Shen, Opt. Lett. 9 (1984) 564.
[64] I.C. Khoo, T.H. Liu, P.Y. Yan, J. Opt. Soc. Am. B 4 (1987) 115.
[65] B.Y. Zeldovich, N. Tabiryan, Zh. Eksp. Teor. Fiz. 82 (1982) 1126 [Sov. Phys. JETP 55 (1982) 656].
[66] E. Brasselet, Phys. Lett. A 323 (2004) 234.
[67] E. Brasselet, L.J. Dube, Phys. Rev. E 73 (2006) 021704.
[68] B. Piccirillo, C. Toscano, F. Vetrano, E. Santamato, Phys. Rev. Lett. 86 (2001) 2285.
[69] B. Piccirillo, A. Vella, E. Santamato, J. Opt. B: Quantum Semiclass Opt. 4 (2002) S20.
[70] L. Marrucci, F. Vetrano, E. Santamato, Opt. Commun. 171 (1999) 131.
[71] B. Piccirillo, A. Vella, E. Santamato, Phys. Rev. E 69 (2004) 021702.
[72] B. Piccirillo, A. Vella, A. Setaro, E. Santamato, Phys. Rev. E 73 (2006) 062701.
[73] F. Lonberg, R.B. Meyer, Phys. Rev. Lett. 55 (1985) 718.
[74] D.W. Allender, R.M. Hornreich, D.L. Johnson, Phys. Rev. Lett. 59 (1987) 2654.
[75] M. Argentina, P. Coullet, E. Risler, Phys. Rev. Lett. 86 (2001) 807.
[76] S. Popp, O. Stiller, I. Aranson, L. Kramer, Physica D 84 (1995) 398.
[77] Y. Kuramoto, Chemical Oscillations, Waves and Turbulence, Springer, Berlin, 1984.
[78] G. Demeter, L. Kramer, unpublished.
[79] P. Coullet, L. Kramer, Chaos 14 (2004) 244.
[80] W.E.L. Hass, J.E. Adams, Appl. Phys. Lett. 25 (1974) 535.
[81] V.G. Bhide, S.C. Jain, S. Chandra, J. Appl. Phys. 48 (1977) 3349.
[82] G. Abbate, P. Maddalena, L. Marrucci, L. Saetta, A. Ferraiuolo, S. Ferraiuolo, E. Santamato, Mol. Cryst. Liq. Cryst. 223 (1992) 11.
[83] G. Abbate, A. Ferraiuolo, P. Maddalena, L. Marrucci, E. Santamato, Liq. Cryst. 14 (1993) 1431.
[84] P. Maddalena, G. Arnone, G. Abbate, L. Marrucci, E. Santamato, Mol. Cryst. Liq. Cryst. 261 (1995) 113.

[85] E. Brasselet, D.O. Krimer, L. Kramer, Europ. Phys. J. E 17 (2005).
[86] D.O. Krimer, E. Brasselet, Phys. Rev., to be published.
[87] G.E. Tsarouhas, J. Ross, J. Chem. Phys. 87 (1988) 5715.
[88] G.E. Tsarouhas, J. Ross, J. Chem. Phys. 89 (1987) 6538.
[89] G. Russo, G. Cipparrone, V. Carbone, Europhys. Lett. 63 (2003) 180.
[90] E. Brasselet, Phys. Rev. E 69 (2004) 021712.
[91] A.E. Miroshnichenko, I. Pinkevych, Y.S. Kivshar, Opt. Express 14 (2006) 2839.